

Intrinsic Sliced Wasserstein Distances for Comparing Collections of Probability Distributions on Manifolds and Graphs

Raif M. Rustamov and Subhabrata Majumdar

Data Science and AI Research, AT&T Chief Data Office, USA

Abstract

Collections of probability distributions arise in a variety of statistical applications ranging from user activity pattern analysis to brain connectomics. In practice these distributions are represented by histograms over diverse domain types including finite intervals, circles, cylinders, spheres, other manifolds, and graphs. This paper introduces an approach for detecting differences between two collections of histograms over such general domains. We propose the intrinsic slicing construction that yields a novel class of Wasserstein distances on manifolds and graphs. These distances are Hilbert embeddable, allowing us to reduce the histogram collection comparison problem to a more familiar mean testing problem in a Hilbert space. We provide two testing procedures one based on resampling and another on combining p -values from coordinate-wise tests. Our experiments in a variety of data settings show that the resulting tests are powerful and the p -values are well-calibrated. Example applications to user activity patterns, spatial data, and brain connectomics are provided.

1 Introduction

Distributional data arise in a variety of statistical applications. In practice these are not limited to distributions over real intervals, but are often defined over manifolds and graphs. For instance, even in the simplest case of analyzing 24-hour activity patterns by constructing histograms of activity counts by time, the resulting histograms are really supported on a circle rather than an interval on the real line. If in addition to the time of activity, the observations come with a real number such as the intensity of the activity, then we end up with a histogram over a cylindrical domain. Spatial datasets recorded at some geographic region level are another example: one can build a distribution over the region adjacency graph by capturing the normalized counts of events in each region. When analyzing distributions over such general domains it is desirable to rely on methods that take into account the connectivity and geometry of the underlying domain, respect the distributional nature of the data, and lead to efficient practical algorithms.

In this paper we consider the problem of comparing two collections of distributions, namely testing for homogeneity—whether all of the distributions come from the same *meta-distribution*. While conceptually similar to two-sample testing, this is a higher order notion in the sense that our units of analysis are distributions/histograms. Letting $\mathcal{P}(\mathcal{X})$ denote the set of distributions on a metric space \mathcal{X} , consider the space $\mathcal{P}(\mathcal{P}(\mathcal{X}))$ of distributions over distributions whose elements we call meta-distributions. Assume that we are given two collections of probability measures $\{\mu_i\}_{i=1}^{N_1}$ and $\{\nu_i\}_{i=1}^{N_2}$ that are drawn from meta-distributions P and Q , $\mu_i \sim P$ and $\nu_i \sim Q$ in an independent and identical manner. Our goal is to test whether $P = Q$ and, moreover, to be able to conduct such tests for general \mathcal{X} . Such a test would be useful in numerous practical situations. For instance, an online retailer may aggregate a customer’s monthly activity into a histogram

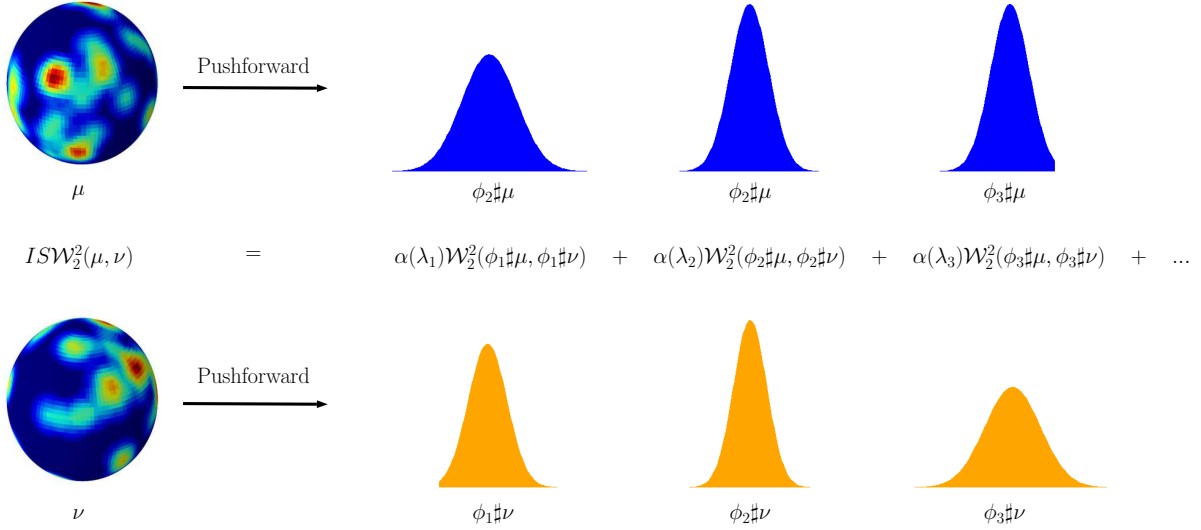


Figure 1: Schematic of the proposed intrinsic slicing construction. Given two probability measures on the sphere (here the darkest blue corresponds to zero mass), different aspects of their dissimilarities become apparent after pushforward to the real line using the eigenfunctions of the Laplace-Beltrami operator, $\{\phi_i\}$, in this case spherical harmonics. As a particular example of our general construction, the (squared) intrinsic sliced 2-Wasserstein distance $ISW_2^2(\cdot, \cdot)$ is the weighted sum of the dissimilarities of the corresponding pushforwards of μ and ν as measured by squared 2-Wasserstein distance $\mathcal{W}_2^2(\cdot, \cdot)$ on the real line.

over a cylinder capturing the time of the day and amount of purchase for each transaction. By considering collections of histograms for various customer segments, one can conduct tests to determine if there are statistically significant differences between behavioral patterns of these segments.

We attack this problem using insights from recent developments that utilize *Hilbert embeddings* for simplifying distributional data problems (see e.g. [2, 41, 32] for particular examples). The simplification comes as a result of linearity of Hilbert spaces, which allows adapting existing statistical approaches such as functional data methodology to distributional data. A crucial requirement on the embedding is that the distance in the embedding space should give a meaningful distance between measures; it is this property that renders quantities computed in the embedding space such as means and variances meaningful. Thus, embedding constructions should be driven by specifying appropriate distances on the space of measures. Of course, not every distance can be embedded and Hilbert embeddable distances are called Hilbertian; see [33] for an overview of this notion.

The focus in this paper will be on transportation based distances between distributions/histograms [43]. Other approaches such as bin-wise treatment of histograms may result in increased variability when horizontal variation is present, leading eventually to less powerful methods. Transportation based distances are more efficient at capturing this and other aspects of distributional data [31, 33, 10]. However, adopting the transportation theoretic approaches to our problem immediately hits a roadblock beyond the real line case: while 2-Wasserstein distance on the real line is Hilbert embeddable, it fails to be so on general domains [33]. The general Hilbert embedding framework of [32] is not tied to a distance between probability distributions and so can be problematic for capturing the location and variability aspects of distribution collections. In addition,

[32] has difficulties in higher dimensions and is not suitable for manifolds or graphs.

Inspired by the sliced 2-Wasserstein distances in high dimensional spaces [26, 25], we introduce a new slicing construction (Figure 1) that leverages the eigenvalues and eigenfunctions of the Laplace-Beltrami operator on manifolds and Laplacian matrices on graphs to capture the intrinsic geometry and connectivity of the domain. We apply this slicing construction to obtain a novel class of intrinsic sliced 2-Wasserstein distances on manifolds and graphs. The resulting distances are Hilbert embeddable, have a number of desirable properties, and can be truncated to obtain finite-dimensional embeddings. Using the corresponding embedding allows us to reduce the histogram collection comparison problem to the comparison of means in a high-dimensional Euclidean space. We provide two approaches for hypothesis testing that take into account the specifics of the problem. The first approach uses bootstrap to compute the null distribution, while the second one avoids resampling. The latter is performed by conducting t -tests on each dimension of the embedding and combining the resulting p -values using recently introduced p -value combination techniques that are robust to dependencies [19, 44, 28]. We verify via extensive experiments on synthetic and real data examples in a variety of data settings that these tests are powerful, and the p -values are well-calibrated.

The paper is organized as follows. We introduce the theoretical machinery for our framework, and go over the rigorous definition of our testing problem in Section 2. To tackle general domains we introduce the intrinsic slicing construction and the resulting distances in Section 3. Our hypothesis testing approach is described in Section 4. Finally, we present simulation results and real data analyses in Sections 5 and 6, respectively. All proofs can be found in the Appendix together with a sample implementation in the R language and additional experiments.

2 Preliminaries

Given a compact metric space \mathcal{X} , let $\mathcal{P}(\mathcal{X})$ denote the set of Borel probability measures on \mathcal{X} . Our main interest is in the case where \mathcal{X} is a graph or a manifold with the shortest/geodesic distance as the metric, and thus the compactness restriction. The 2-Wasserstein distance can be defined on $\mathcal{P}(\mathcal{X})$ using the metric of \mathcal{X} as the ground distance [33, 31], giving $\mathcal{W}_2^{\mathcal{X}} : \mathcal{P}(\mathcal{X}) \times \mathcal{P}(\mathcal{X}) \rightarrow \mathbb{R}_{\geq 0}$; note that we always use \mathcal{W}_2 (without superscript) to denote the 2-Wasserstein distance on the real line. Central to our study are distributions on the space of probability measures $\mathcal{P}(\mathcal{P}(\mathcal{X})) = (\mathcal{P}(\mathcal{X}), \mathcal{B}(\mathcal{P}(\mathcal{X})))$, where $\mathcal{B}(\mathcal{P}(\mathcal{X}))$ is the Borel σ -algebra generated by the topology induced by $\mathcal{W}_2^{\mathcal{X}}$ [10]. Being distributions over distributions, we will refer to the elements of $\mathcal{P}(\mathcal{P}(\mathcal{X}))$ as *meta-distributions*.

Example 1. Consider the case when \mathcal{X} is a discrete space, $\mathcal{X} = \{x_a\}_{a=1}^A$, and so $\mathcal{P}(\mathcal{X}) = \{\sum_a w_a \delta_{x_a} : \sum_a w_a = 1, w_a \geq 0\}$. Any meta-distribution $P \in \mathcal{P}(\mathcal{P}(\mathcal{X}))$ can be described by a probability distribution $p(\mathbf{w})$ over the probability simplex in \mathbb{R}^A . Drawing $\mu \sim P$ is equivalent to drawing the weight vector $[w_1, w_2, \dots, w_A] \sim p(\mathbf{w})$ and setting $\mu = \sum_a w_a \delta_{x_a}$. The case when \mathcal{X} is a graph has the same structure with x_a being the graph nodes. The main difference is that there may be smoothness conditions on the weights of the neighboring nodes—a property that affects the choice of a plausible $p(\mathbf{w})$.

Example 2. Consider the following rather simplistic meta-distribution P describing the daily activity patterns of people. The goal is to assign to every person a probability distribution over a 24-hour circle indicating the probability of them being active (e.g. exercising). To obtain such a $\mu \sim P$, we first draw $c \sim \mathcal{N}(18, 4)\chi_{[6,30]} \bmod 24$ and set $\mu = \mathcal{N}(c, 1)\chi_{[c-12, c+12]} \bmod 24$; here we are using military time, $\chi_{[a,b]}$ is the indicator function, and the distributions are properly

normalized. The idea is that every person has a set exercise time which centers around 18:00 with the standard deviation of 2 hours, and then the actual activity takes place around this center with the standard deviation of 1 hour.

Assume that we are given two collections of probability measures $\{\mu_i\}_{i=1}^{N_1}$ and $\{\nu_i\}_{i=1}^{N_2}$ that are drawn in an independent-and-identically-distributed (hereafter i.i.d.) manner from some meta-distributions P and Q . Our goal is to test the null hypothesis of whether $P = Q$. While this is conceptually a two-sample test, it is a higher order notion since our data points are distributions. In practice, the distributions μ_i or ν_i are given by histograms. Next, we will see that this testing problem can be drastically simplified using appropriate embeddings of probability distributions.

Let $\mathcal{D}(\cdot, \cdot) : \mathcal{P}(\mathcal{X}) \times \mathcal{P}(\mathcal{X}) \rightarrow \mathbb{R}_{\geq 0}$ be a distance between probability distributions. $\mathcal{D}(\cdot, \cdot)$ is called *Hilbertian* if there exist a Hilbert space \mathcal{H} and a map $\eta : \mathcal{P}(\mathcal{X}) \rightarrow \mathcal{H}$ such that $\mathcal{D}(\mu, \nu) = \|\eta(\mu) - \eta(\nu)\|_{\mathcal{H}}$. For example, it is well-known that 2-Wasserstein distance on $\mathcal{X} = \mathbb{R}$ is Hilbertian [33] (also see Example 5) and Maximum Mean Discrepancy (MMD) on any \mathcal{X} is Hilbertian [21]; however, the 2-Wasserstein distance $\mathcal{W}_2^{\mathcal{X}}$ on general \mathcal{X} is not Hilbertian [33].

Since the map η takes every measure on \mathcal{X} to a point in \mathcal{H} , we see that a meta-distribution $P \in \mathcal{P}(\mathcal{P}(\mathcal{X}))$ gives a rise to a measure on \mathcal{H} given by pushforward operation, $\eta \# P = P \circ \eta^{-1} \in \mathcal{P}(\mathcal{H})$. In addition, if a finite dimensional approximation $\eta_D : \mathcal{P}(\mathcal{X}) \rightarrow \mathbb{R}^D$ of η is available, then $\eta_D \# P$ is a measure on \mathbb{R}^D . This observation is enormously useful: problems about the elements of the rather abstract space $\mathcal{P}(\mathcal{P}(\mathcal{X}))$ are reduced to problems about familiar measures on \mathcal{H} or even \mathbb{R}^D . For example, the usual notions of mean and variance can be applied to the measure $\eta \# P$ to gain insights about the meta-distribution P . The validity of these insights hinges on the η -map coming from a Hilbertian distance, as distances are central to the statistical quantities of interest.

Testing for $\eta \# P = \eta \# Q$ can serve as a proxy for our original testing problem of $P = Q$. As typical with two-sample tests, various aspects of the equality $\eta \# P = \eta \# Q$ can be tested, such as the mean or variance equality; unspecific tests of equality can be applied as well. We will concentrate on testing certain aspects of the equality so that one can easily drill down on the results. This is similar to the regular two-sample testing where checking for equality of, say, means is often preferable as it gives immediately interpretable insights, whereas a general test that only says there are unspecified differences between the distributions is less useful for interpretation. Our focus is in line with the recent surge of interest in interpretable learning.

Remark 1. If an unspecific test is desired, Energy Distance based two sample test [42] or the MMD-based test [21] can be adapted by replacing the Euclidean distance between points by a Hilbertian distance \mathcal{D} between the distributions [33]. These tests can be calibrated using the permutation null and will not be discussed further.

To obtain succinct and interpretable tests we will concentrate on the mean of the resulting pushforward measure in \mathcal{H} .

Definition 1. For a meta-distribution $P \in \mathcal{P}(\mathcal{P}(\mathcal{X}))$, we define its *Hilbert centroid* with respect to the Hilbertian distance \mathcal{D} as $C_{\eta \# P} = \mathbb{E}_{\mu \sim P}[\eta(\mu)] \in \mathcal{H}$, assuming it exists.

Our testing procedure is based on checking the equality $C_{\eta \# P} = C_{\eta \# Q}$, or more explicitly: $\mathbb{E}_{\mu \sim P}[\eta(\mu)] = \mathbb{E}_{\nu \sim Q}[\eta(\nu)]$. Intuitively, each “dimension” of the map η probes some aspect of the two involved meta-distributions and makes sure that they are in agreement in expectation. One of our testing approaches will use the statistic

$$\mathbb{T}(P, Q) = \|C_{\eta \# P} - C_{\eta \# Q}\|_{\mathcal{H}}^2 \tag{2.1}$$

to capture the deviations from equality; this quantity can be written directly in terms of pairwise distances.

Proposition 1. *For $P, Q \in \mathcal{P}(\mathcal{P}(\mathcal{X}))$, the following holds:*

$$\mathbb{T}(P, Q) = \mathbb{E}_{\mu \sim P, \nu \sim Q} [\mathcal{D}^2(\mu, \nu)] - \frac{1}{2} \mathbb{E}_{\mu, \mu' \sim P} [\mathcal{D}^2(\mu, \mu')] - \frac{1}{2} \mathbb{E}_{\nu, \nu' \sim Q} [\mathcal{D}^2(\nu, \nu')] \quad (2.2)$$

Different choices of \mathcal{D} and the corresponding η will result in tests that will detect various aspects of deviation from $P = Q$. To clarify this point, we give a few examples of what the equality $C_{\eta \# P} = C_{\eta \# Q}$ implies.

Example 3. Consider the case when \mathcal{X} is a discrete space as in Example 1. Let \mathcal{D} be the ℓ_2 -distance, namely $\mathcal{D}^2(\sum_a w_a \delta_{x_a}, \sum_a w'_a \delta_{x_a}) = \sum_a (w_a - w'_a)^2$. Clearly, the Hilbert map is given by $\eta(\sum_a w_a \delta_{x_a}) = [w_1, w_2, \dots, w_A] \in \mathbb{R}^A$. Using the explicit form of the Hilbert map we see that $C_{\eta \# P} = C_{\eta \# Q}$ holds if and only if the corresponding weight distributions $p(\mathbf{w})$ and $q(\mathbf{w})$ have the same expectations in \mathbb{R}^A . Note that in the related graph example using ℓ_2 -distance is suboptimal as it does not account for the adjacency structure of the graph. In contrast, Wasserstein distances are more appropriate, especially for accounting for horizontal variability as moving weight from a node to its neighbor incurs lower penalty.

Example 4. Let $\mathcal{X} = [0, T] \subset \mathbb{R}$ and consider the following construction of $P \in \mathcal{P}(\mathcal{P}(\mathcal{X}))$ that gives probability distribution functions (pdf) over \mathcal{X} . We draw a function from a Gaussian process $GP(m_P(x), k_P(x, x'))$, clamp its negative values to zero (or take its square, or exponentiate—the goal being to obtain a non-negative function), and normalize to integrate to 1 to obtain a pdf $f : \mathcal{X} \rightarrow \mathbb{R}$. If \mathcal{D} is the L_2 -distance between functions, the Hilbert map η can be taken to be the identity map with $\mathcal{H} = L_2[0, T]$. Thus, the equality $C_{\eta \# P} = C_{\eta \# Q}$ boils down to $\forall x, \mathbb{E}_{f \sim P}[f(x)] = \mathbb{E}_{f \sim Q}[f(x)]$, which would hold true if, for example, the mean functions of the involved Gaussian processes are equal. This type of analysis would be similar to the functional data methodology, but it ignores the fact that probability distributions can potentially be analyzed more efficiently using a wider variety of distances \mathcal{D} such as the Wasserstein distances.

Example 5. Let $\mathcal{X} = [0, T] \subset \mathbb{R}$ with \mathcal{D} being the 2-Wasserstein distance \mathcal{W}_2 . Given a probability measure $\mu \in \mathcal{P}([0, T])$, let F_μ be its cumulative distribution function: $F_\mu(x) = \mu([0, x]) = \int_0^x d\mu$. The generalized inverse of cumulative distribution function (CDF) is defined by $F_\mu^{-1}(s) := \inf\{x \in [0, T] : F_\mu(x) > s\}$. The squared 2-Wasserstein distance has a rather simple expression in terms of the inverse CDF [33]:

$$\mathcal{W}_2^2(\mu, \nu) = \int_0^1 (F_\mu^{-1}(s) - F_\nu^{-1}(s))^2 ds. \quad (2.3)$$

This formula immediately establishes the Hilbertianity of \mathcal{W}_2 through the map $\eta : \mathcal{P}([0, T]) \rightarrow L_2([0, T])$ defined by $\eta(\mu) = F_\mu^{-1}$. Note that η is invertible for increasing normalized functions in the embedding space. Using this insight, we see that the corresponding “average measure” of $P \in \mathcal{P}(\mathcal{P}(\mathcal{X}))$ can be introduced via $P_{\text{av}} = \eta^{-1}(\mathbb{E}_{\mu \sim P}[\eta(\mu)])$. It is easy to prove that P_{av} satisfies the following: $P_{\text{av}} = \arg \min_{\rho \in \mathcal{P}(\mathcal{X})} \mathbb{E}_{\mu \sim P}[\mathcal{W}_2(\mu, \rho)^2]$, which is the definition of the Fréchet mean, see for example [33]. In this setting, $C_{\eta \# P} = C_{\eta \# Q}$ boils down to having the same Fréchet means, $P_{\text{av}} = Q_{\text{av}}$.

Remark 2. While testing for 2-Wasserstein Fréchet mean equality can be contemplated in general domains, there are a number of problems with pursuing such an approach. First, the existence and uniqueness of the Fréchet mean is not guaranteed, and it can be sensitive to small changes.

Second, computing the Fréchet mean is computationally expensive and can become prohibitive when resampling is used to compute the null distribution. Finally, resampling poses conceptual problems: using permutation null will detect differences beyond the equality of Fréchet means, and using bootstrap requires designing the null case, which is highly non-trivial. In contrast, we show that our approach is robust and leads to computationally efficient algorithms.

We will later see that the Hilbert embedding corresponding to the intrinsic sliced 2-Wasserstein distance is assembled of embeddings like in Example 5 applied after pushforwards (see Figure 1 for an intuition). This means that the resulting equality $C_{\eta\#P} = C_{\eta\#Q}$ becomes more stringent, making it a better proxy for detecting the deviations from $P = Q$ without losing the interpretability aspect.

3 Intrinsic Sliced 2-Wasserstein Distance

We introduce a Hilbertian version of \mathcal{W}_2 on manifolds and graphs via a construction we call *intrinsic slicing* due to its use of the domain’s intrinsic geometric properties. To focus our discussion we concentrate on the manifold case, as the graph case is simpler and is obtained by replacing the Laplace-Beltrami operator by the graph Laplacian.

Let $\lambda_\ell, \phi_\ell; \ell = 0, 1, \dots$ be the eigenvalues and eigenfunctions of the Laplace-Beltrami operator on \mathcal{X} with Neumann boundary conditions. The eigenfunctions are sorted by increasing eigenvalue and assumed to be orthonormal with respect to some fixed (e.g. uniform) measure on \mathcal{X} ; also $\phi_0 = \text{const}$ and $\lambda_0 = 0$. One can define a spectral kernel $k(x, y) = \sum_\ell \alpha(\lambda_\ell) \phi_\ell(x) \phi_\ell(y)$ and the corresponding spectral distance on the manifold $d(x, y) = k(x, x) + k(y, y) - 2k(x, y) = \sum \alpha(\lambda_\ell) (\phi_\ell(x) - \phi_\ell(y))^2$, where $\alpha : \mathbb{R}_{\geq 0} \rightarrow \mathbb{R}_{\geq 0}$ is a function that controls contribution from each spectral band. By setting $\alpha(\lambda) = e^{-t\lambda}$ for some $t > 0$, we get the heat/diffusion kernel and the corresponding diffusion distance [15]. Another important case is $\alpha(\lambda) = 1/\lambda^2$ if $\lambda > 0$ and $\alpha(0) = 0$, which gives the biharmonic kernel and distance [27]. In both of these constructions $\alpha(\cdot)$ is a decreasing function, allowing the smoother low-frequency (i.e. smaller λ_ℓ) eigenfunctions to contribute more.

3.1 Definition and properties

A real-valued function $\phi : \mathcal{X} \rightarrow \mathbb{R}$ can be used to map the manifold \mathcal{X} onto the real line. Any probability measure $\mu \in \mathcal{P}(\mathcal{X})$ can likewise be projected onto the real line using the pushforward of ϕ , which we denote by $\phi\#\mu = \mu \circ \phi^{-1} \in \mathcal{P}(\mathbb{R})$. While the pushforward notions used here and in previous sections are conceptually the same, for clarity we use $\#$ for distributions and $\#$ for meta-distributions. We define intrinsic slicing as follows.

Definition 2. Given a function $\alpha : \mathbb{R}_{\geq 0} \rightarrow \mathbb{R}_{\geq 0}$ and a probability distance $\mathcal{D}(\cdot, \cdot)$ on $\mathcal{P}(\mathbb{R})$, we define the intrinsic sliced distance $IS\mathcal{D}(\cdot, \cdot)$ on $\mathcal{P}(\mathcal{X})$ by

$$IS\mathcal{D}^2(\mu, \nu) = \sum_\ell \alpha(\lambda_\ell) \mathcal{D}^2(\phi_\ell\#\mu, \phi_\ell\#\nu). \quad (3.1)$$

The choice of the Laplacian eigenfunctions in the definition can be justified by a number of their properties. Eigenfunctions are intrinsic quantities of a manifold and are ordered by smoothness. Thus, they allow capturing the intrinsic connectivity of the underlying domain. Furthermore, due to the orthogonality of eigenfunctions, their pushforwards can capture complementary aspects of the distribution.

While the definition is general, our focus in this paper is on the case when $\mathcal{D} = \mathcal{W}_2$; we remind that we always use \mathcal{W}_2 to denote the 2-Wasserstein distance on $\mathcal{P}(\mathbb{R})$. We call the resulting distance *Intrinsic Sliced 2-Wasserstein Distance*, and denote it by $IS\mathcal{W}_2$. First, we discuss the convergence of the infinite sum in Definition 2.

Proposition 2. *If \mathcal{X} is a smooth compact n -dimensional manifold and $\sum_{\ell} \lambda_{\ell}^{(n-1)/2} \alpha(\lambda_{\ell}) < \infty$, then $IS\mathcal{W}_2$ is well-defined.*

Next, we prove a number of properties of $IS\mathcal{D}$.

Proposition 3. *If \mathcal{D} is a Hilbertian probability distance such that $IS\mathcal{D}$ is well-defined, then (i) $IS\mathcal{D}$ is Hilbertian, and (ii) $IS\mathcal{D}$ satisfies the following metric properties: non-negativity, symmetry, the triangle inequality, and $IS\mathcal{D}(\mu, \mu) = 0$.*

Proof. By Hilbertian property of \mathcal{D} , there exists a Hilbert space \mathcal{H}^0 and a map $\eta^0 : \mathcal{P}(\mathbb{R}) \rightarrow \mathcal{H}^0$ such that $\mathcal{D}(\rho_1, \rho_2) = \|\eta^0(\rho_1) - \eta^0(\rho_2)\|_{\mathcal{H}^0}$ for all $\rho_1, \rho_2 \in \mathcal{P}(\mathbb{R})$. Plugging this into Eq. (3.1) we have $IS\mathcal{D}(\mu, \nu) = \|\eta(\mu) - \eta(\nu)\|_{\mathcal{H}}$, where $\mathcal{H} = \bigoplus_{\ell} \mathcal{H}^0$ and the ℓ -th component of $\eta(\mu)$ is $\sqrt{\alpha(\lambda_{\ell})} \eta_0(\phi_{\ell} \# \mu) \in \mathcal{H}^0$. The second part of Proposition 3 directly follows from the Hilbert property. \square

Since \mathcal{W}_2 is Hilbertian on $\mathcal{P}(\mathbb{R})$, the application of Proposition 3 yields that $IS\mathcal{W}_2$ is also Hilbertian, making it possible to use $IS\mathcal{W}_2$ for our hypothesis tests in Section 4.

The following result shows that $IS\mathcal{W}_2$ inherits an important property of the Wasserstein distances, namely that the distance between two Dirac delta measures equals to a specific ground distance between their locations.

Proposition 4. *When $\mu = \delta_x(\cdot), \nu = \delta_y(\cdot)$ for two points $x, y \in \mathcal{X}$, we have $IS\mathcal{W}_2(\mu, \nu) = d(x, y)$, where $d(\cdot, \cdot)$ is the spectral distance corresponding to the choice of $\alpha(\cdot)$.*

For a simple choice of distance \mathcal{D} on $\mathcal{P}(\mathbb{R})$, namely the absolute mean difference, the corresponding intrinsic sliced distance is the Maximum Mean Discrepancy(MMD) [21].

Proposition 5. *Let $\mathcal{D}(\rho_1, \rho_2) = |\mathbb{E}_{x \sim \rho_1}[x] - \mathbb{E}_{y \sim \rho_2}[y]|$ for $\rho_1, \rho_2 \in \mathcal{P}(\mathbb{R})$, then the corresponding $IS\mathcal{D}$ is equivalent to the MMD with the spectral kernel $k(\cdot, \cdot)$.*

When $k(x, y)$ is the heat kernel, the sliced distance in Proposition 5 is very much like the MMD with the Gaussian kernel, with the parameter t in $\alpha(\lambda) = e^{-t\lambda}$ controlling the kernel width. Indeed, the two kernels coincide on \mathbb{R}^d , and on general manifolds Varadhan's formula gives asymptotic equivalence for small t [7].

An interesting insight derived from the above result is that $IS\mathcal{W}_2$ is in a sense a “stronger” distance than MMD that uses the corresponding spectral kernel. The $IS\mathcal{W}_2$ compares the quantiles of the pushforward distributions (Eq. (2.3)), whereas MMD compares their expectations only. We formalize this notion in the next result, also providing a theoretical reason for preferring $IS\mathcal{W}_2$ for hypothesis testing.

Proposition 6. *$MMD(\mu, \nu) \leq IS\mathcal{W}_2(\mu, \nu)$ when the same $\alpha(\cdot)$ is used in both constructions.*

Proof. This follows directly from the fact that for $\rho_1, \rho_2 \in \mathcal{P}(\mathbb{R})$ the inequality $|\mathbb{E}_{x \sim \rho_1}[x] - \mathbb{E}_{y \sim \rho_2}[y]| \leq \mathcal{W}_2(\rho_1, \rho_2)$ holds. \square

We are now in a position to prove that $IS\mathcal{W}_2$ is a true metric.

Theorem 1. *If $\alpha(\lambda) > 0$ for all $\lambda > 0$, then $IS\mathcal{W}_2$ is a metric on $\mathcal{P}(\mathcal{X})$.*

We remind that 2-Wasserstein distance can be defined directly on $\mathcal{P}(\mathcal{X})$ using the geodesic distance as the ground metric; we denote this distance as $\mathcal{W}_2^{\mathcal{X}}$. Lipschitz properties of the eigenfunctions imply the following:

Proposition 7. *There exists a constant c depending only on \mathcal{X} such that for all $\mu, \nu \in \mathcal{P}(\mathcal{X})$ the inequality $IS\mathcal{W}_2(\mu, \nu) \leq c\mathcal{W}_2^{\mathcal{X}}(\mu, \nu)\sqrt{\sum_{\ell} \lambda_{\ell}^{(n+3)/2}\alpha(\lambda_{\ell})}$ holds; here, n is the dimension of \mathcal{X} .*

Our final result looks at the quantity \mathbb{T} defined using $IS\mathcal{W}_2$ by Eq. (2.2). We will be using \mathbb{T} computed on finite collections of measures as a test statistic in the next section. We show that it enjoys robustness with respect to small perturbations of the measures in the collection.

Proposition 8. *Let $\{\mu_i\}_{i=1}^N$ and $\{\nu_i\}_{i=1}^N$ be two collections of probability measures on $\mathcal{P}(\mathcal{X})$, such that $\forall i, \mathcal{W}_2^{\mathcal{X}}(\mu_i, \nu_i) \leq \epsilon$, then $\mathbb{T}(\{\mu_i\}_{i=1}^N, \{\nu_i\}_{i=1}^N) \leq C^2\epsilon^2$. Here $C = c\sqrt{\sum_{\ell} \lambda_{\ell}^{(n+3)/2}\alpha(\lambda_{\ell})}$ from previous proposition and is assumed to be finite.*

This bound implies that if the distributions in a collection undergo horizontal shifts that are small as measured by the geodesic distance $\mathcal{W}_2^{\mathcal{X}}$, then \mathbb{T} is small as well.

3.2 Approximate Hilbert Embedding

An important aspect of $IS\mathcal{W}_2$ is that its Hilbert map $\eta : \mathcal{P}(\mathcal{X}) \rightarrow \mathcal{H}$ can be approximated by a finite-dimensional embedding $\eta_D : \mathcal{P}(\mathcal{X}) \rightarrow \mathbb{R}^D$ such that $IS\mathcal{W}_2(\mu, \nu) \approx \|\eta_D(\mu) - \eta_D(\nu)\|_{\mathbb{R}^D}$. This is useful for practical computation and for one of our hypothesis testing approaches.

Using the formula for \mathcal{W}_2 on $\mathcal{P}(\mathbb{R})$ in terms of the quantile function, Eq. (2.3), the Hilbert map is defined by $\eta^0(\mu) = F_{\mu}^{-1}$. We have $\mathcal{W}_2(\mu, \nu) = \|\eta^0(\mu) - \eta^0(\nu)\|_{L_2(\mathbb{R})}$, where the norm involves integration. We can discretize the integral using the Riemann sum; in practice, when working with histograms, higher-order quadrature schemes are not warranted given the jumpy behavior of the integrand. This process can be equivalently seen through the lens of approximating the mapping η^0 . For equidistant knots $s_k = \frac{k}{D'+1}, k = 1, \dots, D'$, define the approximate embedding $\eta_{D'}^0 : \mathcal{P}(\mathbb{R}) \rightarrow \mathbb{R}^{D'}$ as:

$$\eta_{D'}^0 : \mu \rightarrow \frac{1}{\sqrt{D'}}[F_{\mu}^{-1}(s_1), \dots, F_{\mu}^{-1}(s_{D'})]. \quad (3.2)$$

Now, $\mathcal{W}_2(\mu, \nu) \approx \|\eta_{D'}^0(\mu) - \eta_{D'}^0(\nu)\|_{\mathbb{R}^{D'}}$ with approximation quality depending on the embedding dimension D' .

To approximate the Hilbert map for $IS\mathcal{W}_2$ we truncate the series defining $IS\mathcal{W}_2$ and use a finite number of eigenfunctions for pushforwards: $\phi_{\ell}, \ell = 1, \dots, L$, where ϕ_0 is dropped since it is a constant. By inspecting the proof of Proposition 3 and using Eq. (3.2), we can define $\eta_D : \mathcal{P}(\mathcal{X}) \rightarrow \mathbb{R}^D$ with $D = LD'$ as the concatenation of L maps:

$$(\eta_D)_{\ell} : \mu \rightarrow \sqrt{\frac{\alpha(\lambda_{\ell})}{D'}}[F_{\phi_{\ell}\sharp\mu}^{-1}(s_1), \dots, F_{\phi_{\ell}\sharp\mu}^{-1}(s_{D'})].$$

Next subsection provides more details of this computation; in the Appendix we provide an implementation of this embedding in the R language.

3.3 Computational Details

The case of finite intervals is the building block for the general case, so let us first consider the case of $\mathcal{X} = [0, T]$. We represent a histogram over this interval by a discrete measure of the form

\mathcal{X}	Eigenvalues	Eigenfunctions
$[0, T]$	$(\frac{\pi\ell}{T})^2$	$\sqrt{\frac{2}{T}} \cos \frac{\pi\ell x}{T}$
$S^1(T) = [0, T] \bmod T$	$(\frac{2\pi\ell}{T})^2$	$\sqrt{\frac{2}{T}} [\cos / \sin] \frac{2\pi\ell x}{T}$
$[0, T_1] \times [0, T_2]$	$(\frac{\pi\ell_1}{T_1})^2 + (\frac{\pi\ell_2}{T_2})^2$	$\sqrt{\frac{4}{T_1 T_2}} \cos \frac{\pi\ell_1 x}{T_1} \cos \frac{\pi\ell_2 x}{T_2}$
$S^1(T_1) \times [0, T_2]$	$(\frac{2\pi\ell_1}{T_1})^2 + (\frac{\pi\ell_2}{T_2})^2$	$\sqrt{\frac{4}{T_1 T_2}} [\cos / \sin] \frac{2\pi\ell_1 x}{T_1} \cos \frac{\pi\ell_2 x}{T_2}$
$S^1(T_1) \times S^1(T_2)$	$(\frac{2\pi\ell_1}{T_1})^2 + (\frac{2\pi\ell_2}{T_2})^2$	$\sqrt{\frac{4}{T_1 T_2}} [\cos / \sin] \frac{2\pi\ell_1 x}{T_1} [\cos / \sin] \frac{\pi\ell_2 x}{T_2}$
S^2		Spherical harmonics [12]
Graphs/Data Clouds/Meshes		Eigen-decomposition of the Laplacian matrix

Table 1: Eigenvalues and eigenfunctions of the Laplace-Beltrami operator with Neumann boundary conditions for simple manifolds. We exclude zero eigenvalue and the corresponding constant eigenvector; thus, all indices ℓ, ℓ_1, ℓ_2 run over positive integers. The notation $[\cos / \sin]$ means picking either the cosine or sine function—*all choices must be used, giving multiple eigenfunctions*.

$\mu = \sum w_a \delta_{x_a}$ with the histogram bin centers $x_a \in [0, T]$ and weights w_a satisfying $\sum w_a = 1$, where $a = 1, 2, \dots, A$. Note that it is not required for the histograms in the collections to be supported at the same bin locations. For a given histogram, let $\{x_{(a)}, w_{(a)}\}_{a=1}^A$ be the locations sorted from smallest to largest and their corresponding weights; since the bin locations are unique there will not be any ties. The quantile function is computed via $F_\mu^{-1}(s) := \min\{x_{(a)} : \sum_{b \leq a} w_{(b)} > s\}$. The approximate map $\eta_{D'}^0$ now can be computed using the s_k -th quantile value $F_\mu^{-1}(s_k)$ for each value of $s_k, k = 1, \dots, D'$.

For a general domain \mathcal{X} , the histogram representation is the same as above: $\sum w_a \delta_{x_a}$ with the histogram bin centers $x_a \in \mathcal{X}$ and weights w_a satisfying $\sum w_a = 1$, where $a = 1, 2, \dots, A$. The pushforward $\phi_\ell \sharp \mu$ gives a histogram on the real line defined by $\sum w_a \delta_{\phi_\ell(x_a)}$. Note that while x_a are distinct, their images under ϕ_ℓ do not have to be distinct, so one re-aggregates the weights to obtain $\sum_{a \in S} w'_a \delta_{\phi_\ell(x_a)}$, where S is a subset of $1, 2, \dots, A$ and w'_a are the new weights. It is now straightforward to compute the quantile function as before and build the approximate map $(\eta_D)_\ell$. Doing so for the different values of ℓ and concatenating the resulting vectors gives η_D .

In practice, these computations can be carried out on a variety of domains—analytic manifolds, manifolds discretized as point clouds or meshes, and graphs. In most cases the spectral decomposition of the Laplace-Beltrami operator or graph Laplacian has to be computed numerically [15, 36]. For applications that involve simple manifolds, the eigenvalues and eigenfunctions can be computed analytically. For completeness we list them in Table 1. Note that we benefit from the fact that the eigen-decomposition for product spaces can be derived from the eigen-decompositions of the components.

The choice of the function $\alpha(\cdot)$ determining the contributions of each spectral band is problem specific. When working on manifolds of low dimension, the choice of $\alpha(\cdot)$ that corresponds to the biharmonic distance is convenient. While the diffusion distance provides a general choice that works on manifolds of any dimension, the biharmonic distance does not have any parameters to tune and was shown to provide an excellent alternative to the geodesic distance in low-dimensional settings [27]. When in doubt, inspecting the behavior of the distance on the underlying domain will allow assessing whether the distance is appropriate for the given problem. The importance of relying on a well-behaved spectral distance was highlighted in Proposition 4.

4 Hypothesis Testing

Let $\{\mu_i\}_{i=1}^{N_1}$ and $\{\nu_i\}_{i=1}^{N_2}$ be two i.i.d. collections of measures drawn from $P, Q \in \mathcal{P}(\mathcal{P}(\mathcal{X}))$ respectively. Our goal is to use these samples to test the null hypothesis $H_0 : C_{\eta \# P} = C_{\eta \# Q}$, where η is the Hilbert embedding of the sliced distance $IS\mathcal{W}_2$ on $\mathcal{P}(\mathcal{X})$. We propose two nonparametric approaches for testing in Sections 4.1 and 4.2; the former is based on bootstrap and the latter is based on combining the p -values of coordinate-wise tests.

4.1 Resampling Based Test

We use the quantity $\mathbb{T}(\cdot, \cdot)$ from Eq. (2.2) as the test statistic. Its sample version is computed by replacing the expectations by the empirical means, and excluding the diagonal terms to achieve unbiasedness:

$$\hat{\mathbb{T}} \equiv \sum_{i,j} \frac{IS\mathcal{W}_2^2(\mu_i, \nu_j)}{N_1 N_2} - \sum_{i,j:i \neq j} \frac{IS\mathcal{W}_2^2(\mu_i, \mu_j)}{2N_1(N_1 - 1)} - \sum_{i,j:i \neq j} \frac{IS\mathcal{W}_2^2(\nu_i, \nu_j)}{2N_2(N_2 - 1)} \quad (4.1)$$

.

Note that $\mathbb{E}\hat{\mathbb{T}} = \mathbb{T}(P, Q)$. In practice, the $IS\mathcal{W}_2$ values are computed from the approximate embedding: $IS\mathcal{W}_2(\rho_1, \rho_2) \approx \|\eta_D(\rho_1) - \eta_D(\rho_2)\|_{\mathbb{R}^D}$. We denote the resulting statistic by $\tilde{\mathbb{T}}_{L,D'}$.

The difference between $\tilde{\mathbb{T}}_{L,D'}$ and the population version (i.e. $\mathbb{T} - \tilde{\mathbb{T}}_{L,D'}$) can be decomposed as $(\mathbb{T} - \hat{\mathbb{T}}) + (\hat{\mathbb{T}} - \tilde{\mathbb{T}}_L) + (\tilde{\mathbb{T}}_L - \tilde{\mathbb{T}}_{L,D'})$, where the summands inside the terms $\hat{\mathbb{T}}_L$ and $\tilde{\mathbb{T}}_{L,D'}$ correspond to partial sums that approximate $IS\mathcal{W}_2^2(\cdot, \cdot)$ by $\sum_{l=1}^L \alpha(\lambda_l) \mathcal{W}_2^2(\phi_l \sharp \cdot, \phi_l \sharp \cdot)$, and $\mathcal{W}_2^2(\phi_l \sharp \cdot, \phi_l \sharp \cdot)$ by $\|\eta_{D'}(\phi_l \sharp \cdot) - \eta_{D'}(\phi_l \sharp \cdot)\|^2$, respectively. We show in Appendix that a) summands in the second and third terms in the sum can be made infinitesimally small by choosing large enough L and D' , respectively; b) an asymptotic result for the first difference can be obtained using the tools from [21, 40]. These results are based on the following assumptions:

- (i) $\sum_{\ell=1}^{\infty} \alpha(\lambda_{\ell}) \lambda_{\ell}^{(n+3)/2} < \infty$,
- (ii) The pushforward meta-distributions $\eta \# P, \eta \# Q$ are square-integrable: $\mathbb{E}_{\mu, \mu' \sim P} \langle \eta(\mu), \eta(\mu') \rangle_{\mathcal{H}} < \infty$ and $\mathbb{E}_{\nu, \nu' \sim Q} \langle \eta(\nu), \eta(\nu') \rangle_{\mathcal{H}} < \infty$,
- (iii) The meta-distributions P and Q generate absolutely continuous densities.

The first condition is ensured by a suitable choice of the kernel function $\alpha(\cdot)$. For example, given any $t > 0$, the heat kernel $\alpha_t \equiv \alpha(\lambda_{\ell}) = \exp(-t\lambda_{\ell})$, condition (i) is satisfied for all the manifolds listed in Table 1. The third condition is standard in the literature, for example see [32]. The second condition is analogous to those needed to establish Central Limit Theorem (CLT)-like results in probability spaces equipped with the Euclidean metric. For $\mathcal{D} \equiv \mathcal{W}_2$, square-integrable random processes have been considered in recent work—for example, in [8] to perform geodesic PCA on $\mathcal{P}(\mathbb{R})$, and in [9] to compute finite sample risk bounds for Fréchet mean estimates. In our case, this is ensured by the boundedness of the inner product. By definition, $\langle \eta(\mu), \eta(\mu') \rangle_{\mathcal{H}} = \sum_{\ell} \alpha_{\ell} \langle \eta_0(\phi_{\ell} \sharp \mu), \eta_0(\phi_{\ell} \sharp \mu') \rangle_{\mathcal{H}}$. Because of the compactness of \mathcal{X} , Hörmander's bound on the supremum norm of the eigenfunctions can be applied: $\|\phi_{\ell}\|_{\infty} \leq c \lambda_{\ell}^{(n-1)/4} \|\phi_{\ell}\|_2$, for some constant c that depends on the manifold \mathcal{X} . By orthonormality of the eigenfunctions we have $\forall \ell, \|\phi_{\ell}\|_2 = 1$, so the inverse CDF transformation induced by $\eta_0(\phi_{\ell} \sharp \mu) \equiv F_{\phi_{\ell} \sharp \mu}^{-1}$ maps $[0, 1]$ to a bounded interval that is the range of ϕ_{ℓ} . Finally, $\langle \eta(\mu), \eta(\mu') \rangle_{\mathcal{H}} \leq c^2 \sum_{\ell} \alpha_{\ell} \lambda_{\ell}^{(n-1)/2} < \infty$ is ensured by the choice of the kernel function $\alpha(\cdot)$.

Under assumptions (i)-(iii), we establish asymptotic distributions of $\tilde{\mathbb{T}}_{L,D'}$ under both null and alternate hypotheses:

Theorem 2. *Assume conditions (i)-(iii) hold. Define $N = N_1 + N_2$, and suppose that as $N_1, N_2 \rightarrow \infty$, we have $N_1/N \rightarrow \rho_1, N_2/N \rightarrow \rho_2 = 1 - \rho_1$, for some fixed $0 < \rho_1 < 1$. With $L \geq L_N, D' \geq D_N$ chosen in an appropriate way (see Appendix), under $H_0 : C_{\eta \# P} = C_{\eta \# Q}$ we have*

$$N\tilde{\mathbb{T}}_{L,D'} \rightsquigarrow \sum_{m=1}^{\infty} \gamma_m (A_m^2 - 1),$$

where A_m are i.i.d. $\mathcal{N}(0, 1)$ random variables for $m = 1, 2, \dots$, and γ_m are the eigenvalues of a certain operator that depends on P and Q . Further, under $H_1 : C_{\eta \# P} \neq C_{\eta \# Q}$, $\sqrt{N}(\tilde{\mathbb{T}}_{L,D'} - \mathbb{T})$ is asymptotically Gaussian with mean 0 and finite variance.

We evaluate the power performance of the testing procedure based on $\tilde{\mathbb{T}}_{L,D'}$ for the sequence of contiguous alternatives $H_{1N} = \{(P, Q) : C_{\mu \# P} = C_{\mu \# Q} + \delta_N, l = 1, 2, \dots\}$, where the deviation from null is quantified collectively by pushforward differences $\delta_{\ell N} \in \mathcal{H}, \delta_N = \oplus_{\ell}(\sqrt{\alpha_{\ell}} \delta_{\ell N})$ that are made to approach 0 as $N \rightarrow \infty$. The following theorem establishes consistency of our testing procedure against a family of such local alternatives.

Theorem 3. *Assume conditions (i)-(iii) hold, and let L, D' be chosen as in Theorem 2. Then for the sequence of contiguous alternatives H_{1N} such that $N\|\delta_N\|_{\mathcal{H}^*}^2 \rightarrow \infty$, the level- α test based on $\tilde{\mathbb{T}}_{L,D'}$ is consistent for any $\alpha \in (0, 1)$, that is as $N \rightarrow \infty$ the asymptotic power approaches 1.*

A consequence of this result is that as the sample sizes N_1, N_2 grow, our testing procedure is able to detect smaller differences between the Hilbert centroids with high probability.

Testing Procedure In practice, to obtain the p -value for the $\tilde{\mathbb{T}}_{L,D'}$ -statistic we use a bootstrap procedure. Remember that $\tilde{\mathbb{T}}_{L,D'}$ is computed via the approximate embedding η_D with $D = LD'$. The collection $\{\mu_i\}_{i=1}^{N_1}$ is mapped to the collection $\{X_i = \eta_D(\mu_i)\}_{i=1}^{N_1}$ of vectors in \mathbb{R}^D . These can be seen to be i.i.d. from $\eta_D \# P = P \circ \eta_D^{-1} \in \mathcal{P}(\mathbb{R}^D)$. Similarly, for the other collection we have a sample $\{Y_i = \eta_D(\nu_i)\}_{i=1}^{N_2}$ drawn from $\eta_D \# Q$. Now, the null $H_0 : C_{\eta \# P} = C_{\eta \# Q}$ implies that the means of the distributions $\eta_D \# P$ and $\eta_D \# Q$ coincide in \mathbb{R}^D .

The bootstrap null distribution for $\tilde{\mathbb{T}}_{L,D'}$ can be obtained as follows. Let \bar{X} and \bar{Y} be the sample means; construct the combined sample $\{X_i - \bar{X} + \frac{\bar{X} + \bar{Y}}{2}\}_{i=1}^{N_1} \cup \{Y_i - \bar{Y} + \frac{\bar{X} + \bar{Y}}{2}\}_{i=1}^{N_2}$. This centers both samples at $\frac{\bar{X} + \bar{Y}}{2}$. Now, from the combined sample we select with replacement N_1 (resp. N_2) samples to make bootstrap sample $\{X_i^b\}_{i=1}^{N_1}$ (resp. $\{Y_i^b\}_{i=1}^{N_2}$). Repeat this process B times (we take $B = 1000$ in our experiments), and collect the null test statistic values $\tilde{\mathbb{T}}_{L,D'}^b = \tilde{\mathbb{T}}_{L,D'}(\{X_i^b\}_{i=1}^{N_1}, \{Y_i^b\}_{i=1}^{N_2})$ for $b = 1, \dots, B$. The approximate p -value is then given by:

$$p = \frac{1}{B+1} \left(|\{b : \tilde{\mathbb{T}}_{L,D'}^b \geq \tilde{\mathbb{T}}_{L,D'}\}| + 1 \right).$$

Remark 3. Permutation testing cannot be applied in this case as it would detect differences beyond the mean inequality. Such differences help reject the stronger null hypothesis $H_0 : P = Q$ which can be the intent in some situations. However, from point of the view of interpretability, such a rejection will not allow pinpointing the aspect responsible for the difference; a nice discussion can be found in [24]. In a similar context, for hypothesis testing on stochastic processes, [14] previously showed the inability of the permutation procedure to maintain nominal size in the context of independence testing.

4.2 Testing via p -value Combination

The bootstrap test above incurs a high computational cost and the granularity of the p -values is determined by the number of resamples, which can be too coarse in massive multiple comparison settings often seen in industrial applications. Thus, we propose an approach that avoids resampling.

As explained at the end of the previous subsection, testing $H_0 : C_{\eta \# P} = C_{\eta \# Q}$ can be interpreted as testing whether the means of the distributions $\eta_D \# P$ and $\eta_D \# Q$ coincide in \mathbb{R}^D . To this end, we adopt the approach proposed by [39] in a spatial statistics context. First, we apply the Behrens-Fisher-Welch t -test (without assuming equality of variances) to each coordinate of the samples $\{X_i = \eta_D(\mu_i)\}_{i=1}^{N_1}$ and $\{Y_i = \eta_D(\nu_i)\}_{i=1}^{N_2}$ to obtain the p -values $p_k, k = 1, 2, \dots, D$. Second, an overall p -value is computed via the harmonic mean p -value combination method which is robust to dependencies [19, 44]:

$$p^H = H \left(\frac{D}{\frac{1}{p_1} + \frac{1}{p_2} + \dots + \frac{1}{p_D}} \right),$$

where the function H has a known form described in [44]. Another approach for combining p -values is the Cauchy combination test [28], but in our numerical experiments we found that the Cauchy combination approach encounters problems when any of the p -values is very close to 1, which can happen in our setting due to the form of the embedding η_D . Therefore, in contrast to [39], for our problem the harmonic mean combination approach is the only appropriate choice.

Next, we establish that the proposed approach controls the size of the test. Since $\{X_i\}_{i=1}^{N_1}$ can be seen to be i.i.d. from $\eta_D \# P$, we have that the sample mean \bar{X} is asymptotically distributed as the D -dimensional multivariate normal distribution $\mathcal{N}(C_{\eta_D \# P}, \text{Cov}[\eta_D \# P]/N_1)$. Indeed, due to the compactness of the underlying space \mathcal{X} and the way η_D is constructed, the image of the embedding η_D is a bounded subset of \mathbb{R}^D . Thus, the Central Limit Theorem [11] can be used to deduce the asymptotic normality. Due to independence of the samples, we have:

$$\bar{X} - \bar{Y} \sim \mathcal{N} \left(C_{\eta_D \# P} - C_{\eta_D \# Q}, \frac{\text{Cov}[\eta_D \# P]}{N_1} + \frac{\text{Cov}[\eta_D \# Q]}{N_2} \right).$$

Our goal is to test for $H_0 : C_{\eta_D \# P} = C_{\eta_D \# Q}$, i.e. if the mean of the above distribution is zero.

This observation has two consequences. First, this validates the use of coordinate-wise t -tests as the requirement of asymptotic normality is satisfied for each coordinate. Second, computing t -statistics involves only the estimation of the diagonal of the covariance matrix, $\text{diag}(\Sigma)$. As a result, $Z = (\bar{X} - \bar{Y})/\sqrt{\text{diag}(\Sigma)}$ is not only asymptotically multivariate normal, but approximately so even for moderate values of sample sizes N_1 and N_2 .

The following result establishes control for size; this is a version of Theorem 1 from [28] but for harmonic mean combination p -value. Assume that a test statistic $Z \in \mathbb{R}^D$ has null distribution with zero mean and every pair of coordinates of Z follows bivariate normal distribution. Compute the coordinate-wise two-sided p -values $p_k = 2(1 - \Phi(|Z_k|))$ for $k = 1, 2, \dots, D$, where Φ is the standard normal cumulative distribution function. The following approximation holds; a proof can be found in the Appendix.

Theorem 4. *Let $p_k, k = 1, \dots, D$ be the null p -values as above and p^H computed via harmonic mean approach, then*

$$\lim_{\alpha \rightarrow 0} \frac{\text{Prob}\{p^H \leq \alpha\}}{\alpha} = 1.$$

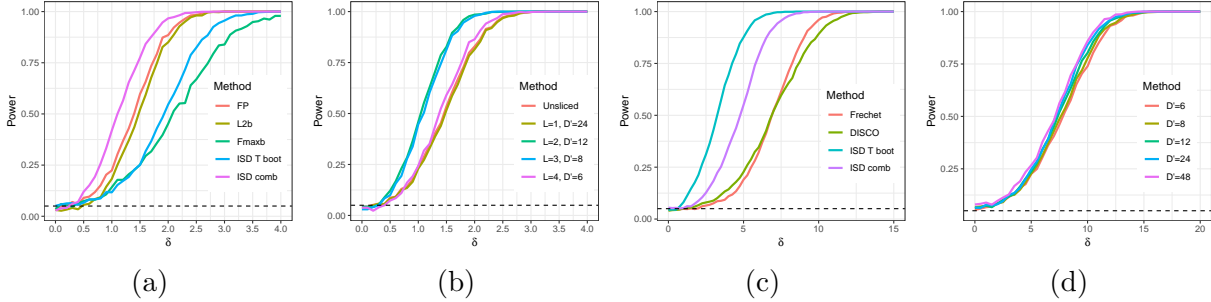


Figure 2: Performance on synthetic finite interval and manifold data. Finite interval: (a) comparison with existing methods—a test based on basis function representation (FP) [20], a sum-type ℓ_2 norm-based test (L2b) [45], and a max-type test [46] that uses the maximum of coordinate-wise F statistic (Fmaxb); (b) unsliced vs. different settings of (L, D') . Manifold data: (c) circular data, comparing with Fréchet ANOVA [17], and the DISCO nonparametric test [37]; (d) harmonic combination tests on cylindrical data for $L = 4$. Dotted lines indicates nominal size of all tests ($\alpha = 0.05$).

This theorem can be readily applied in our setting; the bivariate normality is the consequence of the multivariate normality. Of course, our coordinate-wise p -values are computed using the appropriate t -distributions, but the difference between these and the standard normal is negligible when sample sizes are large. As a result, the proposed procedure asymptotically controls for the size of the test for small values of the level α . Our experimental results show that the control is already achieved for moderate sample sizes and the commonly used $\alpha = 0.05$.

Remark 4. A major benefit of the p -value combination approach is that the resulting test is *interpretable*. Since the coordinates of the η_D -embeddings correspond to quantiles in the pushforwards, one can find and study the coordinates that exhibit the most difference to obtain further insights about the dissimilarity between the groups.

5 Synthetic Experiments

We compare the performance of our tests on data from a number of domains with several existing methods, and settings of the embedding parameters L, D' . For evaluation, we use empirical power at different degrees of departure from the null hypothesis, calculated by averaging the proportion of rejections at level $\alpha = 0.05$ over 1000 independent datasets with samples divided into two groups of sizes $n_1 = 60, n_2 = 40$. To ensure the tests are well-calibrated, we also calculate nominal sizes assuming the two sample groups are drawn from the same random meta-distribution. We calculate eigenvalues and eigenfunctions using analytical expressions provided in the Appendix, and fix $\alpha(\lambda) = e^{-\lambda}$ (i.e. heat kernel with $t = 1$) for all experiments.

Finite intervals To obtain our base measures μ_i, ν_i , we generate bin probabilities as (shifted and normalized) values of the function $f(t_j) = \mu(t_j) + \alpha(t_j)$ at $m = 30$ fixed design points $t_j = j/(m+1), j = \{1, 2, \dots, m\}$, and

$$\begin{aligned}\mu(t_j) &= 1.2 + 2.3 \cos(2\pi t_j) + 4.2 \sin(2\pi t_j), \\ \alpha(t_j) &= \epsilon_0 + \sqrt{2}\epsilon_1 \cos(2\pi t_j) + \sqrt{3}\epsilon_2 \sin(2\pi t_j),\end{aligned}$$

where $\epsilon_0, \epsilon_1, \epsilon_2 \sim N(0, 1)$ clipped between $[-3, 3]$. Group 1 and 2 samples are obtained as $\mu_i(\cdot) \equiv f(\cdot)$ and $\nu_i(\cdot) \equiv f(\cdot) + \delta$ respectively, where $\delta \in [0, 4]$ is a constant. To make the sample functions non-negative, we shift all functions by $M = 3(1 + \sqrt{2} + \sqrt{3})$. Finally, as the m -length vector of bin counts for a sample, we generate a random vector from the Multinomial distribution with 1000 trials, m outcomes and the outcome probabilities proportional to the shifted functional observations corresponding to that sample.

We use embedding dimensions $L = 3, D' = 10$ to compare our method against 11 functional ANOVA tests—for brevity we report results for 3 of them which use different methodological approaches (see Appendix for complete results). All methods maintain nominal size for $\delta = 0$ (Figure 2 a). While the combination test (ISD comb) based on our proposal outperformed all the other tests across all values of δ , the bootstrap test that uses the overall \mathbb{T} statistic (ISD T boot) performs better than Fmaxb but worse than others.

We also compare the p -value combination test based on an *unsliced* 24-dimensional inverse CDF embedding with sliced ISW_2 -based tests (Figure 2 b). We use multiple pairs of (L, D') values, all of them giving overall embeddings of dimension $D = LD' = 24$. The performance of an ISW_2 -based test that uses slicing over only the first eigenfunction is almost as good as the unsliced version. With more eigenfunctions, the powers first improve considerably, then become similar to the unsliced version again.

Manifold domains We consider data from distributions on circles and cylinders. For circular data, we take von Mises distributions with randomly chosen parameters as our samples. For an angle x (measured in radians), the von Mises probability density function is given by $f(x|\mu, \kappa) = \exp[\kappa \cos(x - \mu)](2\pi I_0(\kappa))^{-1}$, where $I_0(\kappa)$ is the modified Bessel function of order 0. We fix $\kappa = 2$, and use $\mu \equiv \mu_i \sim N(0, 0.1^2)$, $\mu \equiv \nu_i \sim N(\delta, 0.1^2)$ for samples from group 1 and 2 respectively—with $\delta \in [0, 15] \times \pi/180$ (i.e. 0 to 15 degrees converted to radians). As each observation vector, we take 100 random draws from each sample-specific distribution. For our embeddings, we use $L = 10, D' = 20$, and so our final embedding dimension is $10 \times 20 \times 2 = 400$. Since the competing methods cannot handle circular geometry directly, to implement them we cut the circle into an interval. Figure 2 (c) shows that all methods maintain nominal size, but both our tests maintain considerably higher power than existing methods for all δ .

We generate cylindrical data in the form of samples of a bivariate random vector (Θ, X) , using the cylindrical density function proposed by [29]:

$$f(\theta, x) = \frac{e^{\kappa \cos(\theta - \mu)}}{2\pi I_0(\kappa)} \frac{1}{\sqrt{2\pi\sigma_c^2}} e^{-\frac{(x - \mu_c)^2}{2\sigma_c^2}},$$

clipping values of the X -coordinate between the bounded interval $[0, 2\pi]$. This distribution has the parameters $\mu \in [-\pi, \pi], \mu_0 \in \mathbb{R}, \kappa \geq 0, \rho_1 \in [0, 1], \rho_2 \in [0, 1], \sigma > 0$, where μ, κ denote parameters for the (circular) marginal along the Θ -coordinate. and given $\Theta = \theta$, X is sampled from $N(\mu_c, \sigma_c^2)$, with

$$\begin{aligned} \mu_c &= \mu + \sqrt{\kappa\sigma} \{ \rho_1(\cos \theta - \cos \mu) + \rho_2(\sin \theta - \sin \mu) \}, \\ \sigma_c &= \sigma^2(1 - \rho^2), \rho = (\rho_1^2 + \rho_2^2)^{1/2}. \end{aligned}$$

In our experiments, we fix $\rho_1 = \rho_2 = 0.5, \sigma = 1, \kappa = 2$ across both populations. As random samples of distributions, we draw $\mu, \mu_0 \sim \text{Unif}(0, 1)$ and $\mu, \mu_0 \sim \text{Unif}(\delta, \delta + 1)$ for samples of group 1 and 2 respectively, with $n_1 = 60, n_2 = 40$. We repeat the above for $\delta \in [0, 30]$ degrees converted to radians, and obtain bivariate histograms corresponding to each sample distribution

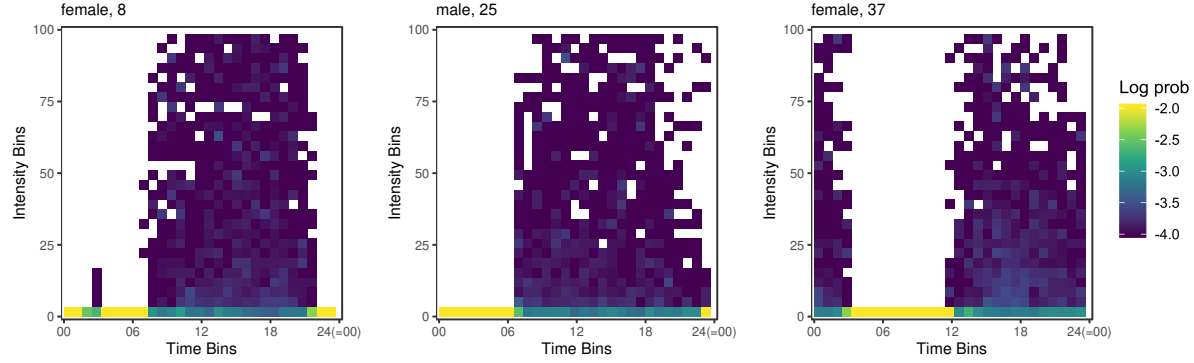


Figure 3: Activity histograms for three individuals from NHANES dataset. There are 100 bins in the intensity and 96 in the time dimension; we show hour of day on the time axis. The time dimension is periodic where 00:00 is identified with 24:00, giving rise to a cylindrical histogram domain.

from 500 random draws from that distribution. To evaluate the effects of choosing L, D' we calculate our embeddings for $L \in \{2, 3, 4, 5\}$, $D' \in \{6, 8, 12, 24, 48\}$. The choice of L has small effect on performance, so we report results for $L = 4$ in Figure 2 (d). Higher values of D' result in some increase in power.

6 Real Data

6.1 NHANES data on physical activity monitoring

As our first real data application, we analyze the Physical Activity Monitor (PAM) data from the 2005-2006 National Health and Nutrition Examination Survey (NHANES)¹. This contains physical activity pattern readings for a large number of people collected over 1 week period on a per-minute granularity. After basic pre-processing steps to ensure no missing entries, as well as data reliability and well-calibrated activity monitors, we use data from 6839 individuals. The data for each individual corresponds to device intensity value from the PAM for $24 \times 60 = 1440$ minutes throughout the day, for 7 days.

For each individual we can capture their activity patterns into a cylindrical histogram with time and intensity dimensions. For each observation, its time during the day is discretized into 15-minute intervals giving 96 bins for the time dimension; its intensity value (capped at 1,000) is discretized into a 100 equidistant bins. Since the time dimension is periodic, we obtain a histogram over the cylinder $S^1(T_1) \times [0, T_2]$, with $T_1 = 96$, $T_2 = 100$. Normalized counts can thus be considered as person-specific probability distributions; several examples are shown in Figure 3. Note that flattening the domain by cutting the cylinder will arbitrarily split activity patterns (see especially Figure 3, Female 37) and will lead to inefficiencies due to horizontal variability.

We apply the proposed methodology to check if the activity patterns vary across different groups of individuals obtained as follows. We first split the overall dataset based on the individual's age using the following inclusive ranges: 6–15, 16–25, ..., 76–85; this covers all the ages in the dataset. From each split we sample 100 males and 100 females to avoid gender imbalance driving the results. Thus, we end up with 8 age groups with 200 individuals per group. Our goal is to compare these 8 groups' activity patterns by conducting pair-wise tests.

¹https://www.cdc.gov/Nchs/Nhanes/2005-2006/PAXRAW_D.htm

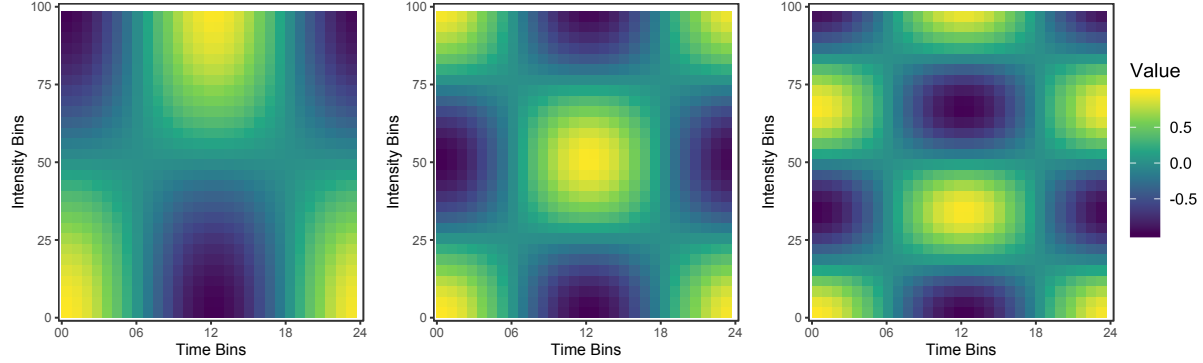


Figure 4: Three eigenfunctions for the NHANES histogram domain normalized by the maximum absolute value. Note that the eigenfunctions are periodic in the time direction (i.e. match when glued over the side cut) but not in the intensity direction, reflecting the cylindrical geometry of the underlying domain.

Age Groups	6–15	16–25	26–35	36–45	46–55	56–65	66–75	76–85
6–15		0.979	0.31	0.383	0.297	0.905	0.921	0.326
16–25	3.7e-11		0.998	0.963	0.443	0.872	0.442	0.529
26–35	4.6e-20	1.0e-05		0.987	0.818	0.93	0.731	0.992
36–45	3.2e-26	3.5e-11	0.01		0.945	0.984	0.974	0.327
46–55	6.6e-27	8.4e-16	0.002	0.377		0.832	0.618	0.844
56–65	2.4e-32	7.5e-20	3.1e-04	0.042	0.977		0.509	0.98
66–75	5.4e-45	1.6e-16	7.7e-06	1.6e-04	0.001	0.011		0.557
76–85	3.4e-52	1.4e-23	1.4e-15	2.7e-12	9.7e-16	1.4e-09	2.1e-06	

Table 2: Comparing the activity intensity of different age groups based on the NHANES dataset. Below diagonal: p -values corresponding to the actual data comparisons. Above diagonal: null p -values obtained by combining and randomly splitting the two involved groups. The entries in boldface correspond to the rejected hypotheses with the BH procedure at the FDR level of 0.1.

To perform our analysis we compute the eigenvalues and eigenfunctions as per the 4th row of Table 1 using $\ell_1 = 1, 2, 3$ and $\ell_2 = 1, 2, 3$, giving a total of $L = 2 \times 3 \times 3 = 18$ eigenfunctions; three of the resulting eigenfunctions are shown in Figure 4. We consider a $D' = 5$ dimensional embedding for the inverse CDF transformation, hence the final embedding dimension after the slicing construction is $D = LD' = 18 \times 5 = 90$.

We summarize the results in Table 2, *below the diagonal*. The p -values are obtained via the harmonic mean combination approach. We run the Benjamini-Hochberg [6] procedure on the resulting p -values at the false discovery rate of 0.1, and the rejected hypotheses are indicated by the p -values in bold. Our method detects statistically significant differences between all pairs of groups, except 46–55 versus 36–45 and 56–65 groups. As a control experiment, we provide our method with null cases and display the p -values in Table 2, *above the diagonal*. The null cases are obtained by combining the individuals from the two comparison groups and splitting it arbitrarily (i.e. mixing the two age groups). As expected, the p -values of the control comparisons do not concentrate near zero.

Curiously, our method can be used “off-label” to conduct *functional data analyses* over different

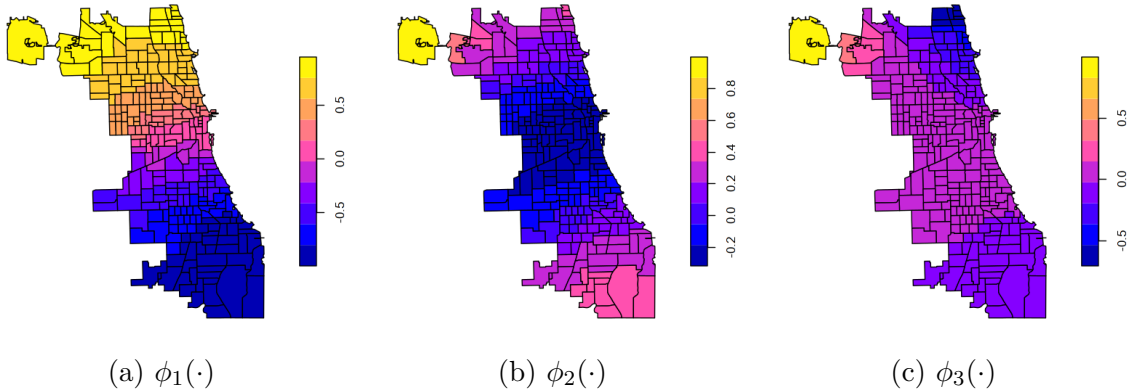


Figure 5: First three eigenvectors of the Laplacian are shown for the beat adjacency graph, mapped back to the geographic locations. All of the eigenvectors are normalized by the maximum absolute value. The spatial smoothness of the eigenvectors—somewhat masked here due to the discrete colormap—is crucial to efficiently capturing horizontal variability of the data (i.e. distribution shifts over the graph). The boundaries of beats are shown based on the shape file from Chicago Data portal.

dimensions of the NHANES dataset. For example, one can concentrate on a single day of activity intensity data which gives a curve over the 24-hour circle. Since activity intensity is a non-negative number, these curves can be normalized so as to obtain probability distributions. Now we can use our methodology to detect pair-wise differences across groups. While this has the benefit of accounting for underlying geometry of data, it loses the absolute magnitude information due to the normalization. Clearly the appropriateness of such an analysis would depend on the goal of the exercise and the particular research question attached to that goal; our proposal provides a framework that is flexible enough to handle data of different modalities.

6.2 Chicago Crime

We demonstrate the use of our methodology on histograms over graphs. In this experiment, we use the Chicago Crimes 2018 dataset² which captures incidents of crime in the City of Chicago. We base our analysis on the type of crime, the beat (geographic area subdivision used by police, see Figure 5) where the incident took place, and the date of the incident. To capture the spatial aspect of the data we build a graph with one vertex per beat; two vertices are connected by an edge if the corresponding beats share a geographic boundary. For each crime type and day, we capture the total count of that crime type for each beat; after normalizing this gives a daily probability distribution over the graph. Our goal is to compare the collection of distributions of, say, theft occurring on Tuesday to those of Thursday and Saturday. The Tuesday versus Thursday comparison is intended as a null case, as we do not expect to see any differences between them [39].

We build the un-normalized Laplacian of the beat adjacency graph, and compute its lowest frequency $L = 20$ eigenvalues and eigenvectors. The first three eigenvectors are plotted in Figure 5. The number of inverse CDF values used in the embedding is $D' = 5$, which gives rise to $D = 100$ dimensional embedding. The results of comparisons are shown in the last two columns of Table 3; the p -values are obtained via the harmonic mean combination approach. We run the

²data.cityofchicago.org

Crime Type	Tuesday		Thursday		Saturday		Tue vs Thu	Tue vs Sat
	<i>N</i>	count	<i>N</i>	count	<i>N</i>	count	<i>p</i> -value	<i>p</i> -value
Theft	52	178.7	52	182.9	52	180.2	0.452	4.7e-06
Deceptive Practice	51	55.8	52	54.9	52	44.4	0.255	4.2e-04
Battery	52	125.8	52	123.0	52	154.9	0.374	0.001
Robbery	50	25.2	50	25.1	52	28.1	0.130	0.002
Narcotics	51	36.0	51	34.6	50	36.9	0.890	0.008
Criminal Damage	52	70.0	52	73.7	52	83.0	0.901	0.03
Other Offense	52	49.5	52	48.4	52	44.1	0.670	0.037
Burglary	52	34.0	52	33.1	52	29.1	0.157	0.183
Motor Vehicle Theft	52	27.9	52	26.2	51	28.1	0.923	0.365
Assault	52	57.2	52	59.3	52	52.4	0.996	0.617

Table 3: Results on Chicago Crime 2018 dataset. The entries in bold correspond to the rejected hypotheses with the BH procedure at the FDR level of 0.1. The *N* column captures the number of days passing the filtering criteria, and the count column shows the average per-day crime count.

Benjamini-Hochberg [6] procedure on the 20 resulting *p*-values at the false discovery rate of 0.1, and the rejected hypotheses are indicated by the *p*-values in bold. As expected, no differences were detected between Tuesday and Thursday patterns. On the other hand, we see that there are statistically significant differences between Tuesday and Saturday patterns in the following categories of crime: theft, deceptive practice, battery, robbery, narcotics, and criminal damage.

6.3 Brain Connectomics

In this example, we consider two publicly available brain connectomics datasets [1, 3] distributed as a part of the R package `graphclass`³. Both are based on resting state functional magnetic resonance imaging (fMRI): COBRE has data on 54 schizophrenics and 70 controls, and UMich with 39 schizophrenics and 40 controls. The datasets capture the pairwise correlations between 264 regions of interest (ROI) of Power parcellation [34] and can be considered as a 264 node graph (263 nodes for COBRE as ROI 75 is missing) with positive and negative edge weights.

We define three probability measures supported on the nodes of the graph. For each ROI we take the sum of absolute values of all its correlations with the remaining ROIs. Now we have a positive number assigned to each node capturing its overall connectivity to the rest of the graph and we normalize to obtain a measure; this construction will be referred to as “all correlations”. Note that each scanned subject gives rise to a separate “all correlations” probability measure on the same underlying node set. The “positive correlations” and “negative correlations” constructions are based on keeping respectively only positive or only negative correlations and aggregating as above.

We also need a fixed base graph for the computation of the Laplacian eigen-decomposition; this graph should capture the spatial connectivity of the ROIs which is relevant due to the smooth nature of the blood oxygenation level dependent (BOLD) signal that is used for computing the correlations. To this end, we obtain the coordinates for the centers of the 264 ROIs⁴ and build the base graph by connecting each ROI to its nearest 8 ROIs. We compute the lowest frequency

³<http://github.com/jesusdaniel/graphclass>

⁴www.jonathanpower.net/2011-neuron-bigbrain.html

Dataset	All correlations	Positive correlations	Negative correlations
COBRE	0.0084	0.00019	0.0019
UMich	0.609	0.116	0.022

Table 4: Comparison results between the schizophrenic and control groups for brain connectomics datasets.

$L = 20$ eigenvalues and eigenvectors of the corresponding un-normalized Laplacian. The number of inverse CDF values used in the embedding is $D' = 5$, which gives rise to $D = 100$ dimensional embedding.

Table 4 shows the result of comparing the schizophrenic group to the control group for both of the datasets; the p -values are obtained via the harmonic mean combination approach. We can see that our approach detects statistically significant differences between the two groups in COBRE dataset in all of the three types of measures on graphs. In contrast, for UMich dataset, the difference is detected only in the negative correlations and loses significance when corrected for multiple testing. This is potentially caused by the higher inhomogeneity of the UMich dataset that was pooled across five different experiments spanning seven years [3]. An interesting aspect of our analysis is that due to normalization (to obtain probability measures) the total sum of connectivity is factored out by the proposed method. As a result, the detected differences are not related to the well-known change in the overall connectivities between the two groups, but rather to distributional changes in marginal connectivity strengths.

7 Conclusion

We have introduced an approach for detecting differences in the behaviors of random collections of probability distributions. Our experiments confirm that the resulting tests are powerful and the p -values are well-calibrated. Several applications to real world data have been presented. Our approach is valid on general domains such as manifolds and graphs, thanks to the general nature of the Intrinsic Sliced 2-Wasserstein distance proposed in this paper.

Several straightforward developments have been omitted from our presentation to maintain the focus. First, hypothesis tests to detect differences between three or more collections of histograms can be developed. Indeed, since our p -value combination test is based on mean comparisons, under suitable assumptions we can instead of t -tests perform an ANOVA F -test for differences among means and combine the resulting p -values as before. Second, by a similar argument it would be possible to perform paired samples tests to compare repeated observations from the same sample. Third, one can replace the means appearing in our tests by weighted means. Thus, different samples or sample groups may be assigned different weights to perform a general weighted hypothesis test—such as differentially weighing female and male samples while comparing different age groups in the NHANES example. Depending on the application, these weights may correspond to the accuracy of observations from the sample distributions [5], or selection bias due to confounding factors.

The construction of ISW_2 provides a novel embedding of probability distributions into a Hilbert space. This can be used to adapt many inferential methods to general spaces where the existence of Fréchet means or higher moments are not guaranteed. The ISW_2 can also be useful for machine learning applications where prediction targets live in a general domain. Given that rigorous Fréchet mean-based methodology for such problems has only been proposed recently [22],

development of prediction models for manifold-valued data that are free of restrictive assumptions is an attractive future line of research.

References

- [1] C. J. Aine, H. J. Bockholt, J. R. Bustillo, J. M. Cañive, A. Caprihan, C. Gasparovic, F. M. Hanlon, J. M. Houck, R. E. Jung, J. Lauriello, J. Liu, A. R. Mayer, N. I. Perrone-Bizzozero, S. Posse, J. M. Stephen, J. A. Turner, V. P. Clark, and Vince D. Calhoun. Multimodal neuroimaging in schizophrenia: Description and dissemination. *Neuroinformatics*, 15(4):343–364, Oct 2017.
- [2] David Applegate, Tamraparni Dasu, Shankar Krishnan, and Simon Urbanek. Unsupervised clustering of multidimensional distributions using earth mover distance. In *Proceedings of the 17th ACM SIGKDD International Conference on Knowledge Discovery and Data Mining*, KDD ’11, pages 636–644, New York, NY, USA, 2011. Association for Computing Machinery.
- [3] Jesús D. Arroyo Relión, Daniel Kessler, Elizaveta Levina, and Stephan F. Taylor. Network classification with applications to brain connectomics. *Ann. Appl. Stat.*, 13(3):1648–1677, 09 2019.
- [4] N. S. Bakhvalov. On the approximate calculation of multiple integrals. *J. Complexity*, 31:502–516, 2015. English translation; the original appeared in *Vestnik MGU, Ser. Math. Mech. Astron. Phys. Chem*, 4, 3–18, 1959.
- [5] A. Bellot and M. van der Schaar. Kernel Hypothesis Testing with Set-valued Data. <https://arxiv.org/abs/1907.04081>, 2020.
- [6] Yoav Benjamini and Yosef Hochberg. Controlling the false discovery rate: A practical and powerful approach to multiple testing. *Journal of the Royal Statistical Society. Series B (Methodological)*, 57(1):289–300, 1995.
- [7] M. Berger. *A Panoramic View of Riemannian Geometry*. Springer-Verlag Berlin Heidelberg, 2003.
- [8] J. Bigot, R. Gouet, T. Klein, and A. López. Geodesic PCA in the Wasserstein space by convex PCA. *Ann. Inst. Henri Poincaré Probab. Stat.*, 53:1–26, 2017.
- [9] J. Bigot, R. Gouet, T. Klein, and A. López. Upper and lower risk bounds for estimating the Wasserstein barycenter of random measures on the real line. *Electron. J. Stat.*, 12:2253–2289, 2018.
- [10] Jérémie Bigot. Statistical data analysis in the wasserstein space. *ESAIM: ProcS*, 68:1–19, 2020.
- [11] Patrick Billingsley. *Probability and measure*. Wiley, New York, third edition, 1995.
- [12] Brett Borden and James Luscombe. *Essential Mathematics for the Physical Sciences*, volume Volume I: Homogeneous boundary value problems, Fourier methods, and special functions, chapter Spherical harmonics and friends. Morgan & Claypool Publishers, 2017. Pages 6–1 to 6–26.

- [13] L. Brown and S. Steinerberger. On the Wasserstein distance between classical sequences and the Lebesgue measure. *Trans. Amer. Math. Soc.*, in press, 2020. <https://arxiv.org/abs/1909.09046>.
- [14] K. Chwialkowski and A. Gretton. A Kernel Independence Test for Random Processes. In *ICML-2014*, volume 32 of \mathcal{Z} , pages 1422–1430, 2014.
- [15] Ronald R. Coifman and Stéphane Lafon. Diffusion maps. *Applied and Computational Harmonic Analysis*, 21(1):5 – 30, 2006. Special Issue: Diffusion Maps and Wavelets.
- [16] Herold Dehling and Roland Fried. Asymptotic distribution of two-sample empirical U-quantiles with applications to robust tests for shifts in location. *Journal of Multivariate Analysis*, 105(1):124–140, 2012.
- [17] Paromita Dubey and Hans-Georg Müller. Fréchet analysis of variance for random objects. *Biometrika*, 106(4):803–821, 10 2019.
- [18] N. Gavish, P. Nyquist, and M. Peletier. Large deviations and gradient flows for the Brownian one-dimensional hard-rod system. <https://arxiv.org/abs/1909.02054>, 2019.
- [19] I. J. Good. Significance tests in parallel and in series. *Journal of the American Statistical Association*, 53(284):799–813, 1958.
- [20] T. Gorecki and L. Smaga. A Comparison of Tests for the One-Way ANOVA Problem for Functional Data. *Computational Statistics*, 30:987–1010, 2015.
- [21] Arthur Gretton, Karsten M. Borgwardt, Malte J. Rasch, Bernhard Schölkopf, and Alexander Smola. A kernel two-sample test. *J. Mach. Learn. Res.*, 13:723–773, March 2012.
- [22] Kyunghee Han, Hans-Georg Müller, and Byeong U. Park. Additive functional regression for densities as responses. *Journal of the American Statistical Association*, 115:997–1010, 2020.
- [23] Jingchen Hu, Yiqian Shi, and Bin Xu. The gradient estimate of a neumann eigenfunction on a compact manifold with boundary. *Chinese Annals of Mathematics, Series B*, 36(6):991–1000, Nov 2015.
- [24] Yifan Huang, Haiyan Xu, Violeta Calian, and Jason C. Hsu. To permute or not to permute. *Bioinformatics*, 22(18):2244–2248, 07 2006.
- [25] Soheil Kolouri, Kimia Nadjahi, Umut Simsekli, Roland Badeau, and Gustavo Rohde. Generalized sliced wasserstein distances. In H. Wallach, H. Larochelle, A. Beygelzimer, F. Alché-Buc, E. Fox, and R. Garnett, editors, *Advances in Neural Information Processing Systems 32*, pages 261–272. Curran Associates, Inc., 2019.
- [26] Soheil Kolouri, Phillip E. Pope, Charles E. Martin, and Gustavo K. Rohde. Sliced wasserstein auto-encoders. In *7th International Conference on Learning Representations, ICLR 2019, New Orleans, LA, USA, May 6-9, 2019*. OpenReview.net, 2019.
- [27] Yaron Lipman, Raif M. Rustamov, and Thomas A. Funkhouser. Biharmonic distance. *ACM Trans. Graph.*, 29(3), July 2010.
- [28] Yaowu Liu and Jun Xie. Cauchy combination test: A powerful test with analytic p-value calculation under arbitrary dependency structures. *Journal of the American Statistical Association*, 115(529):393–402, 2020.

[29] K. V. Mardia and T. W. Sutton. A Model for Cylindrical Variables with Applications. *Journal of the Royal Statistical Society: Series B (Methodological)*, 40(2):229–233, 1978.

[30] Charles A. Micchelli, Yuesheng Xu, and Haizhang Zhang. Universal kernels. *J. Mach. Learn. Res.*, 7:2651–2667, December 2006.

[31] Victor M. Panaretos and Yoav Zemel. Statistical aspects of wasserstein distances. *Annual Review of Statistics and Its Application*, 6(1):405–431, 2019.

[32] Alexander Petersen and Hans-Georg Müller. Functional data analysis for density functions by transformation to a hilbert space. *Ann. Statist.*, 44(1):183–218, 02 2016.

[33] Gabriel Peyré and Marco Cuturi. Computational optimal transport: With applications to data science. *Foundations and Trends in Machine Learning*, 11(5-6):355–607, 2019.

[34] Jonathan D. Power, Alexander L. Cohen, Steven M. Nelson, Gagan S. Wig, Kelly Anne Barnes, Jessica A. Church, Alecia C. Vogel, Timothy O. Laumann, Fran M. Miezin, Bradley L. Schlaggar, and Steven E. Petersen. Functional network organization of the human brain. *Neuron*, 72(4):665–678, Nov 2011. 22099467[pmid].

[35] M. Reed and B. Simon. *Methods of modern mathematical physics. Vol. 1: Functional Analysis*. Academic Press, 1080.

[36] Martin Reuter, Franz-Erich Wolter, Martha Shenton, and Marc Niethammer. Laplace-Beltrami eigenvalues and topological features of eigenfunctions for statistical shape analysis. *Computer-Aided Design*, 41(10):739–755, 2009.

[37] M. L. Rizzo and G. J. Székely. DISCO analysis: A nonparametric extension of analysis of variance. *Ann. Appl. Stat.*, 4:1034–1055, 2010.

[38] Yossi Rubner, Carlo Tomasi, and Leonidas J. Guibas. The earth mover’s distance as a metric for image retrieval. *International Journal of Computer Vision*, 40(2):99–121, 2000.

[39] Raif M. Rustamov and James T. Klosowski. Kernel mean embedding based hypothesis tests for comparing spatial point patterns. *Spatial Statistics*, 38:100459, 2020.

[40] R. J. Serfling. *Approximation theorems of mathematical statistics*. John Wiley & Sons, 2009.

[41] Justin Solomon, Raif M. Rustamov, Leonidas J. Guibas, and Adrian Butscher. Wasserstein propagation for semi-supervised learning. In *Proceedings of the 31th International Conference on Machine Learning, ICML 2014, Beijing, China, 21-26 June 2014*, volume 32 of *JMLR Workshop and Conference Proceedings*, pages 306–314. JMLR.org, 2014.

[42] Gábor J. Székely and Maria L. Rizzo. A new test for multivariate normality. *Journal of Multivariate Analysis*, 93(1):58 – 80, 2005.

[43] Cédric Villani. *Topics in optimal transportation*. Graduate studies in mathematics. American mathematical society, Providence, Rhode Island, 2003.

[44] Daniel J. Wilson. The harmonic mean p-value for combining dependent tests. *Proceedings of the National Academy of Sciences*, 116(4):1195–1200, 2019.

[45] J.-T. Zhang. *Analysis of Variance for Functional Data*. Chapman and Hall/CRC, first edition, 2013.

[46] J.-T. Zhang, M.-Y. Chen, H.-T. Wu, and B. Zhou. A new test for functional one-way ANOVA with applications to ischemic heart screening. *Computational Statistics & Data Analysis*, 132:3–17, 2019.

A Proofs of Theorems and Additional Notes

A.1 Proofs and Notes for Section 2

Remark 5. Here we contrast our testing setup with the traditional two-sample testing. Consider $P \in \mathcal{P}(\mathcal{P}(\mathcal{X}))$ constructed as follows. Let $\mu^* \in \mathcal{P}(\mathcal{X})$ be a fixed probability measure. Let $x_1, x_2, \dots, x_A \sim \mu^*$ and construct the histogram summarizing this sample: $\frac{1}{A} \sum_{a=1}^A \delta_{x_a}$. Now, $\frac{1}{A} \sum_{a=1}^A \delta_{x_a} \in \mathcal{P}(\mathcal{X})$ is one sample drawn from P . In our testing scenario one gets the collection $\{\mu_i\}_{i=1}^{N_1}$, where each histogram is obtained as above: $\mu_i \sim P$. Similarly, consider $Q \in \mathcal{P}(\mathcal{P}(\mathcal{X}))$ of the same type based on some other fixed $\nu^* \in \mathcal{P}(\mathcal{X})$, and let $\{\nu_i\}_{i=1}^{N_2}$ the corresponding collection of histograms. Testing whether $P = Q$ in the limit boils down to $\mu^* = \nu^*$. When compared to the usual two-sample testing this may seem rather inefficient, requiring A times more samples (resp. $N_1 A$ and $N_2 A$ samples from μ^* and ν^*). However, in our setup it is *not assumed* that the histograms in the collections come from meta-distributions of the above simple type (i.e. all μ_i are generated by drawing from the same underlying distribution μ^*). In fact, the target use-case for our approach is when these histograms are collected by observing different individuals who have their *person-specific* behaviors/distributions as in Example 2.

Proposition 1. *For $P, Q \in \mathcal{P}(\mathcal{P}(\mathcal{X}))$, the following equality holds:*

$$\mathbb{T}(P, Q) = \mathbb{E}_{\mu \sim P, \nu \sim Q} [\mathcal{D}^2(\mu, \nu)] - \frac{1}{2} \mathbb{E}_{\mu, \mu' \sim P} [\mathcal{D}^2(\mu, \mu')] - \frac{1}{2} \mathbb{E}_{\nu, \nu' \sim Q} [\mathcal{D}^2(\nu, \nu')], \quad (\text{A.1})$$

where to avoid notational clutter we use $\mathcal{D}^2(\cdot, \cdot)$ as a shorthand for $(\mathcal{D}(\cdot, \cdot))^2$.

Proof. This is a straightforward application of the “kernel trick”: using the Hilbert property of the distance we can rewrite,

$$\begin{aligned} & \mathbb{E}_{\mu \sim P, \nu \sim Q} [\|\eta(\mu) - \eta(\nu)\|_{\mathcal{H}}^2] - \frac{1}{2} \mathbb{E}_{\mu, \mu' \sim P} [\|\eta(\mu) - \eta(\mu')\|_{\mathcal{H}}^2] - \frac{1}{2} \mathbb{E}_{\nu, \nu' \sim Q} [\|\eta(\nu) - \eta(\nu')\|_{\mathcal{H}}^2] \\ &= \mathbb{E}_{\mu \sim P} [\|\eta(\mu)\|_{\mathcal{H}}^2] + \mathbb{E}_{\nu \sim Q} [\|\eta(\nu)\|_{\mathcal{H}}^2] - 2 \langle \mathbb{E}_{\mu \sim P} [\eta(\mu)], \mathbb{E}_{\nu \sim Q} [\eta(\nu)] \rangle_{\mathcal{H}} \\ & \quad - \mathbb{E}_{\mu \sim P} [\|\eta(\mu)\|_{\mathcal{H}}^2] - \mathbb{E}_{\nu \sim Q} [\|\eta(\nu)\|_{\mathcal{H}}^2] \\ & \quad + \langle \mathbb{E}_{\mu \sim P} [\eta(\mu)], \mathbb{E}_{\mu \sim P} [\eta(\mu)] \rangle_{\mathcal{H}} + \langle \mathbb{E}_{\nu \sim Q} [\eta(\nu)], \mathbb{E}_{\nu \sim Q} [\eta(\nu)] \rangle_{\mathcal{H}} \\ &= \|\mathbb{E}_{\mu \sim P} [\eta(\mu)] - \mathbb{E}_{\nu \sim Q} [\eta(\nu)]\|_{\mathcal{H}}^2 = \mathbb{T}(P, Q). \end{aligned}$$

Which gives the sought equivalence. \square

A.2 Proofs and Notes for Section 3

Proposition 2. *If \mathcal{X} is a smooth compact n -dimensional manifold and $\sum_{\ell} \lambda_{\ell}^{(n-1)/2} \alpha(\lambda_{\ell}) < \infty$, then ISW_2 is well-defined.*

Proof. We use Hörmander’s bound on the supremum norm of the eigenfunctions:

$$\|\phi_{\ell}\|_{\infty} \leq c \lambda_{\ell}^{(n-1)/4} \|\phi_{\ell}\|_2,$$

for some constant c that depends on the manifold. By orthonormality of the eigenfunctions we have $\forall \ell, \|\phi_{\ell}\|_2 = 1$. Next, note that $\mathcal{W}_2(\phi_{\ell} \# \mu, \phi_{\ell} \# \nu) \leq 2 \|\phi_{\ell}\|_{\infty}$ as the maximum distance that the mass would be transported in any transportation plan involving pushforwards via ϕ_{ℓ} is upper

bounded by $2\|\phi_\ell\|_\infty$. As a result, every term in the series defining $IS\mathcal{W}_2$ can be upper-bounded by the terms of the following series:

$$\sum_\ell 4\|\phi_\ell\|_\infty^2 \alpha(\lambda_\ell) \leq \sum_\ell 4c^2 \lambda_\ell^{(n-1)/2} \alpha(\lambda_\ell) \propto \sum_\ell \lambda_\ell^{(n-1)/2} \alpha(\lambda_\ell),$$

which proves the claim by the direct comparison test for convergence of series. \square

Remark 6. When Weyl law applies, we have that $\lambda_\ell = \Theta(\ell^{2/n})$, which allows us to replace the above condition by $\sum_\ell \ell^{(n-1)/n} \alpha(\lambda_\ell) < \infty$. For the diffusion kernel/distance choice of $\alpha(\lambda) = e^{-t\lambda}$ the series always converges independently of the manifold dimension. For biharmonic choice of $\alpha(\lambda) = 1/\lambda^2$, the sufficient condition is the convergence of $\sum_\ell \ell^{(n-1)/n} / \lambda_\ell^2 \sim \sum_\ell \ell^{(n-1)/n} / (\ell^{2/n})^2 = \sum_\ell \ell^{(n-5)/n}$, where we applied Weyl's asymptotic again. As a result, the biharmonic choice of α is guaranteed to provide a well-defined $IS\mathcal{W}_2$ for 1 and 2-dimensional manifolds. Notice, however, that the Hörmander's bound used in the proof of the above proposition can be rather lax in some of the settings that are practically relevant, such as the product spaces of lines and circles (where all of the eigenfunctions are bounded by a constant as can be seen from Table 1), and, thus, convergence for the biharmonic choice holds more widely.

Proposition 3. *If \mathcal{D} is a Hilbertian probability distance such that $IS\mathcal{D}$ is well-defined, then*

- (i) $IS\mathcal{D}$ is Hilbertian, and
- (ii) $IS\mathcal{D}$ satisfies the following metric properties: non-negativity, symmetry, the triangle inequality, and $IS\mathcal{D}(\mu, \mu) = 0$.

Proof. By Hilbertian property of \mathcal{D} , there exists a Hilbert space \mathcal{H}^0 and a map $\eta^0 : \mathcal{P}(\mathbb{R}) \rightarrow \mathcal{H}^0$ such that $\mathcal{D}(\rho_1, \rho_2) = \|\eta^0(\rho_1) - \eta^0(\rho_2)\|_{\mathcal{H}^0}$ for all $\rho_1, \rho_2 \in \mathcal{P}(\mathbb{R})$. Plugging this into the definition of $IS\mathcal{D}$ we have $IS\mathcal{D}(\mu, \nu) = \|\eta(\mu) - \eta(\nu)\|_{\mathcal{H}}$, where $\mathcal{H} = \bigoplus_\ell \mathcal{H}^0$ and the ℓ -th component of $\eta(\mu)$ is $\sqrt{\alpha(\lambda_\ell)} \eta_0(\phi_\ell \sharp \mu) \in \mathcal{H}^0$. The second part of Proposition 3 directly follows from the Hilbert property. \square

Proposition 4. *When $\mu = \delta_x(\cdot), \nu = \delta_y(\cdot)$ for two points $x, y \in \mathcal{X}$, we have $IS\mathcal{W}_2(\mu, \nu) = d(x, y)$, where $d(\cdot, \cdot)$ is the spectral distance corresponding to the choice of $\alpha(\cdot)$.*

Proof. We have $\phi_\ell \sharp \delta_x = \delta_{\phi_\ell(x)}$ and similarly for y . Now $\mathcal{W}_2^2(\phi_\ell \sharp \mu, \phi_\ell \sharp \nu) = \mathcal{W}_2^2(\delta_{\phi_\ell(x)}, \delta_{\phi_\ell(y)}) = (\phi_\ell(x) - \phi_\ell(y))^2$. This last equality follows from the fact that the 2-Wasserstein on real line between delta measures is equal to the distance between the two points. Then scaling and adding up gives exactly the kernel distance $d(x, y)$ between the two points. \square

Proposition 5. *Let $\mathcal{D}(\rho_1, \rho_2) = |\mathbb{E}_{x \sim \rho_1}[x] - \mathbb{E}_{y \sim \rho_2}[y]|$ for $\rho_1, \rho_2 \in \mathcal{P}(\mathbb{R})$, then the corresponding intrinsic sliced distance is equivalent to the MMD with the spectral kernel $k(\cdot, \cdot)$.*

Proof. We can rewrite the definition as follows:

$$\begin{aligned} IS\mathcal{D}^2(\mu, \nu) &= \sum_\ell \alpha(\lambda_\ell) (\mathbb{E}_{x \sim \phi_\ell \sharp \mu}[x] - \mathbb{E}_{y \sim \phi_\ell \sharp \nu}[y])^2 = \sum_\ell \alpha(\lambda_\ell) (\mathbb{E}_{x \sim \mu}[\phi_\ell(x)] - \mathbb{E}_{y \sim \nu}[\phi_\ell(y)])^2 \\ &= \sum_\ell \alpha(\lambda_\ell) (\mathbb{E}_{x, x' \sim \mu}[\phi_\ell(x)\phi_\ell(x')] + \mathbb{E}_{y, y' \sim \nu}[\phi_\ell(y)\phi_\ell(y')] - 2\mathbb{E}_{x \sim \mu, y \sim \nu}[\phi_\ell(x)\phi_\ell(y)]) \\ &= \mathbb{E}_{x, x' \sim \mu} \left[\sum_\ell \alpha(\lambda_\ell) \phi_\ell(x)\phi_\ell(x') \right] + \mathbb{E}_{y, y' \sim \nu} \left[\sum_\ell \alpha(\lambda_\ell) \phi_\ell(y)\phi_\ell(y') \right] \\ &\quad - 2\mathbb{E}_{x \sim \mu, y \sim \nu} \left[\sum_\ell \alpha(\lambda_\ell) \phi_\ell(x)\phi_\ell(y) \right] \\ &= \mathbb{E}_{x, x' \sim \mu}[k(x, x')] + \mathbb{E}_{y, y' \sim \nu}[k(y, y')] - 2\mathbb{E}_{x \sim \mu, y \sim \nu}[k(x, y)], \end{aligned}$$

where we used the spectral kernel $k(x, y) = \sum_{\ell} \alpha(\lambda_{\ell}) \phi_{\ell}(x) \phi_{\ell}(y)$. The last expression coincides with the MMD based on kernel $k(\cdot, \cdot)$; see Lemma 6 in [21]. \square

Proposition 6. $MMD(\mu, \nu) \leq ISW_2(\mu, \nu)$ when the same $\alpha(\cdot)$ is used in both constructions.

Proof. This follows directly from the fact that for $\rho_1, \rho_2 \in \mathcal{P}(\mathbb{R})$ the inequality $|\mathbb{E}_{x \sim \rho_1}[x] - \mathbb{E}_{y \sim \rho_2}[y]| \leq \mathcal{W}_1(\rho_1, \rho_2) \leq \mathcal{W}_2(\rho_1, \rho_2)$ holds. Here the first inequality follows from the centroid bound [38], and the second inequality is the well-known ordering property of Wasserstein distances [43]. \square

Theorem 1. If $\alpha(\lambda) > 0$ for all $\lambda > 0$, then ISW_2 is a metric on $\mathcal{P}(\mathcal{X})$.

Proof. In the light of the Proposition 3 it remains only to prove that $ISW_2(\mu, \nu) = 0$ implies $\mu = \nu$. According to Proposition 6, $ISW_2(\mu, \nu) = 0$ yields $MMD(\mu, \nu) = 0$. The assumption that $\alpha(\lambda) > 0$ for all $\lambda > 0$ implies that the spectral kernel $k(\cdot, \cdot)$ corresponding to $\alpha(\cdot)$ is universal [30]. Universality implies the characteristic property [21], which in turn means that $MMD(\mu, \nu) = 0$ is equivalent to $\mu = \nu$, proving the claim. \square

Proposition 7. There exists a constant c depending only on \mathcal{X} such that for all $\mu, \nu \in \mathcal{P}(\mathcal{X})$ the inequality $ISW_2(\mu, \nu) \leq c\mathcal{W}_2^{\mathcal{X}}(\mu, \nu) \sqrt{\sum_{\ell} \lambda_{\ell}^{(n+3)/2} \alpha(\lambda_{\ell})}$ holds; here, n is the dimension of \mathcal{X} .

Proof. We remind $\mathcal{W}_2^{\mathcal{X}}$ is the 2-Wasserstein distance defined directly $\mathcal{P}(\mathcal{X})$ using the geodesic distance as the ground metric. The Neumann eigenfunctions on compact manifolds satisfy the inequality $\|\nabla \phi_{\ell}\|_{\infty} \leq c_1 \lambda_{\ell} \|\phi_{\ell}\|_{\infty}$, see [23]. Applying the bound used in the proof of convergence, $\|\phi_{\ell}\|_{\infty} \leq c_2 \lambda_{\ell}^{(n-1)/4}$, we get that ϕ_{ℓ} is Lipschitz with respect to the geodesic distance on \mathcal{X} with the Lipschitz constant bounded by $c \lambda_{\ell} \lambda_{\ell}^{(n-1)/4} = c \lambda_{\ell}^{(n+3)/4}$.

Consider the optimal coupling between μ and ν whose cost equals to $\mathcal{W}_2^{\mathcal{X}}(\mu, \nu)$. Note that this coupling straightforwardly provides a coupling between the pushforwards $\phi_{\ell\#}\mu$ and $\phi_{\ell\#}\nu$. Using the Lipschitz property of eigenfunctions, we see that the cost of the pushforward coupling is smaller than $c \lambda_{\ell}^{(n+3)/4} \mathcal{W}_2^{\mathcal{X}}(\mu, \nu)$. Since any such coupling provides an upper bound on $\mathcal{W}_2(\phi_{\ell\#}\mu, \phi_{\ell\#}\nu)$, we have $\mathcal{W}_2(\phi_{\ell\#}\mu, \phi_{\ell\#}\nu) \leq c \lambda_{\ell}^{(n+3)/4} \mathcal{W}_2^{\mathcal{X}}(\mu, \nu)$. Plugging this into the formula for ISW_2 we get the claimed bound. \square

Proposition 8. Let $\{\mu_i\}_{i=1}^N$ and $\{\nu_i\}_{i=1}^N$ be two collections of probability measures on $\mathcal{P}(\mathcal{X})$, such that $\forall i, \mathcal{W}_2^{\mathcal{X}}(\mu_i, \nu_i) \leq \epsilon$, then $\mathbb{T}(\{\mu_i\}_{i=1}^N, \{\nu_i\}_{i=1}^N) \leq C^2 \epsilon^2$. Here $C = c \sqrt{\sum_{\ell} \lambda_{\ell}^{(n+3)/2} \alpha(\lambda_{\ell})}$ from previous proposition and is assumed to be finite.

Proof. We have

$$\begin{aligned} \mathbb{T}(\{\mu_i\}_{i=1}^N, \{\nu_i\}_{i=1}^N) &= \left\| \frac{1}{N} \sum_{i=1}^N \eta(\mu_i) - \frac{1}{N} \sum_{i=1}^N \eta(\nu_i) \right\|_{\mathcal{H}}^2 = \left\| \frac{1}{N} \sum_{i=1}^N (\eta(\mu_i) - \eta(\nu_i)) \right\|_{\mathcal{H}}^2 \\ &\leq \frac{1}{N} \sum_{i=1}^N \|\eta(\mu_i) - \eta(\nu_i)\|_{\mathcal{H}}^2 = \frac{1}{N} \sum_{i=1}^N ISW_2^2(\mu_i, \nu_i) \leq \frac{1}{N} \sum_{i=1}^N (C \mathcal{W}_2^{\mathcal{X}}(\mu_i, \nu_i))^2 \\ &\leq \frac{1}{N} N (C \epsilon)^2 = C^2 \epsilon^2. \end{aligned}$$

\square

A.3 Proofs and Notes for Section 4.1

We remind that we will be using the following test statistic for the results that are discussed below:

$$\hat{\mathbb{T}} \equiv \sum_{i,j} \frac{IS\mathcal{W}_2^2(\mu_i, \nu_j)}{N_1 N_2} - \sum_{i,j: i \neq j} \frac{IS\mathcal{W}_2^2(\mu_i, \mu_j)}{2N_1(N_1 - 1)} - \sum_{i,j: i \neq j} \frac{IS\mathcal{W}_2^2(\nu_i, \nu_j)}{2N_2(N_2 - 1)}. \quad (\text{A.2})$$

Proposition 9. *Assume conditions (i)-(iii) hold. Define $N = N_1 + N_2$, and assume that as $N_1, N_2 \rightarrow \infty$, we have $N_1/N \rightarrow \rho_1, N_2/N \rightarrow \rho_2 = 1 - \rho_1$, for some fixed $0 < \rho_1 < 1$. Define a new measure R as a scaled mixture of the centered pushforward measures*

$$R = \left(\frac{1}{\rho_1} + \frac{1}{\rho_2} \right)^{-1} \left[\frac{1}{\rho_1} (\eta \# P - C_{\eta \# P}) + \frac{1}{\rho_2} (\eta \# Q - C_{\eta \# Q}) \right] = \rho_2 (\eta \# P - C_{\eta \# P}) + \rho_1 (\eta \# Q - C_{\eta \# Q}).$$

Suppose $\gamma_m, m = 1, 2, \dots$ are the eigenvalues of

$$\frac{1}{\rho_1 \rho_2} \int_{\mathcal{H}} \langle x, x' \rangle_{\mathcal{H}} \psi_m(x') dR(x') = \gamma_m \psi_m(x).$$

Then under $H_0 : C_{\eta \# P} = C_{\eta \# Q}$ we have

$$N \hat{\mathbb{T}} \sim \sum_{m=1}^{\infty} \gamma_m (A_m^2 - 1), \quad (\text{A.3})$$

where A_m are i.i.d. $\mathcal{N}(0, 1)$ random variables. Under $H_1 : C_{\eta \# P} \neq C_{\eta \# Q}$ we have $\sqrt{N}(\hat{\mathbb{T}} - \mathbb{T}) \sim N(0, \sigma_1^2)$, where

$$\begin{aligned} \sigma_1^2 = & 4 \left[\frac{1}{\rho_1} \mathbb{V}_{\mu \sim P} \mathbb{E}_{\mu' \sim P} \langle \eta(\mu), \eta(\mu') \rangle_{\mathcal{H}} + \frac{1}{\rho_2} \mathbb{V}_{\nu \sim Q} \mathbb{E}_{\nu' \sim Q} \langle \eta(\nu), \eta(\nu') \rangle_{\mathcal{H}} + \right. \\ & \left. \frac{1}{\rho_1} \mathbb{V}_{\mu \sim P} \mathbb{E}_{\nu \sim Q} \langle \eta(\mu), \eta(\nu) \rangle_{\mathcal{H}} + \frac{1}{\rho_2} \mathbb{V}_{\nu \sim Q} \mathbb{E}_{\mu \sim P} \langle \eta(\mu), \eta(\nu) \rangle_{\mathcal{H}} \right]. \end{aligned} \quad (\text{A.4})$$

Remark 7. Note that while this may seem similar to the result of [21], there is an important difference. While [21] has the null hypothesis of $H_0 : P = Q$, our null hypothesis is weaker $H_0 : C_{\eta \# P} = C_{\eta \# Q}$ and requires a somewhat different proof approach.

Proof. Using the Hilbertianity of $IS\mathcal{D}$ (Proposition 3), we have

$$\begin{aligned} IS\mathcal{D}^2(\mu_i, \mu_j) &= \|\eta(\mu_i) - \eta(\mu_j)\|_{\mathcal{H}}^2 \\ &= \|\eta(\mu_i)\|_{\mathcal{H}}^2 + \|\eta(\mu_j)\|_{\mathcal{H}}^2 - 2 \langle \eta(\mu_i), \eta(\mu_j) \rangle_{\mathcal{H}}, \end{aligned}$$

and consequently,

$$\sum_{i,j: i \neq j} IS\mathcal{D}^2(\mu_i, \mu_j) = 2(N_1 - 1) \sum_{i=1}^{N_1} \|\eta(\mu_i)\|_{\mathcal{H}}^2 - 2 \sum_{i,j: i \neq j} \langle \eta(\mu_i), \eta(\mu_j) \rangle_{\mathcal{H}}.$$

Similarly,

$$\begin{aligned} \sum_{i,j: i \neq j} IS\mathcal{D}^2(\nu_i, \nu_j) &= 2(N_2 - 1) \sum_{i=1}^{N_2} \|\eta(\nu_i)\|_{\mathcal{H}}^2 - 2 \sum_{i,j: i \neq j} \langle \eta(\nu_i), \eta(\nu_j) \rangle_{\mathcal{H}}, \\ \sum_{i,j} IS\mathcal{D}^2(\mu_i, \nu_j) &= N_2 \sum_{i=1}^{N_1} \|\eta(\mu_i)\|_{\mathcal{H}}^2 + N_1 \sum_{j=1}^{N_2} \|\eta(\nu_j)\|_{\mathcal{H}}^2 - 2 \sum_{i,j: i \neq j} \langle \eta(\mu_i), \eta(\nu_j) \rangle_{\mathcal{H}}. \end{aligned}$$

Putting these back into Eq. (A.2) after simplifying and cancelling out the norm-square terms we have

$$\begin{aligned}\hat{\mathbb{T}} = & \frac{1}{N_1(N_1-1)} \sum_{i,j:i \neq j} \langle \eta(\mu_i), \eta(\mu_j) \rangle_{\mathcal{H}} + \frac{1}{N_2(N_2-1)} \sum_{i,j:i \neq j} \langle \eta(\nu_i), \eta(\nu_j) \rangle_{\mathcal{H}} \\ & - \frac{2}{N_1 N_2} \sum_{i,j} \langle \eta(\mu_i), \eta(\nu_j) \rangle_{\mathcal{H}}.\end{aligned}\tag{A.5}$$

At this point, we replace the maps η by their centered versions $\tilde{\eta}(\mu) = \eta(\mu) - C_{\eta \# P}$, $\tilde{\eta}(\nu) = \eta(\nu) - C_{\eta \# Q}$; remember that the center of mass of $\eta \# P$ is denoted by $C_{\eta \# P}$. Accumulating the sample-level partial sums above the centering terms cancel out under $H_0 : C_{\eta \# P} = C_{\eta \# Q}$, so that each η can be replaced by $\tilde{\eta}$ in (A.5) above.

Denote $x_i \equiv \tilde{\eta}(\mu_i)$, $y_i \equiv \tilde{\eta}(\nu_i)$ as the Hilbert-embedded samples of $X \sim \tilde{\eta} \# P$, $Y \sim \tilde{\eta} \# Q$, respectively. We remind now that R is a mixture of the centered pushforward measures: $R = \rho_2(\tilde{\eta} \# P) + \rho_1(\tilde{\eta} \# Q)$. Let $L_2(\mathcal{H}, R)$ be the space of real-valued functions on \mathcal{H} that are square integrable with respect to R . Now we can define the following operator $S : L_2(\mathcal{H}, R) \rightarrow \mathcal{H}$,

$$(Sf)(x) := \int_{\mathcal{H}} \langle x, x' \rangle_{\mathcal{H}} f(x') dR(x').$$

Following condition (ii), $\langle \cdot, \cdot \rangle_{\mathcal{H}}$ is square-integrable under R . The above operator is thus Hilbert-Schmidt, hence compact [35, Theorem VI.23]. Consequently, it permits an eigenfunction decomposition with respect to measure R , $\langle x, x' \rangle_{\mathcal{H}} = \sum_{m=1}^{\infty} \gamma_m \psi_m(x) \psi_m(x')$, for $x, x' \in \mathcal{H}$. Note that here $\psi_m : \mathcal{H} \rightarrow \mathbb{R}$ and

$$\int_{\mathcal{H}} \langle x, x' \rangle_{\mathcal{H}} \psi_m(x') dR(x') = \gamma_m \psi_m(x),$$

$$\int_{\mathcal{H}} \psi_m(x) \psi_n(x) dR(x) = \delta_{mn}.$$

Due to the centering of η we also have when $\gamma_m \neq 0$,

$$\gamma_m \mathbb{E}_X[\psi_m(x)] = \int_{\mathcal{H}} \mathbb{E}_X[\langle x, x' \rangle_{\mathcal{H}}] \psi_m(x') dR(x') = 0 \Rightarrow \mathbb{E}_X[\psi_m(x)] = 0.$$

Similarly, $\mathbb{E}_Y[\psi_m(y)] = 0$. The V-statistic from the overall sample can now be written as an infinite sum [40, Section 5.5]:

$$\|\hat{C}_{\eta \# P} - \hat{C}_{\eta \# Q}\|_{\mathcal{H}}^2 = \sum_{m=1}^{\infty} \gamma_m \left(\frac{1}{N_1} \sum_{i=1}^{N_1} \psi_m(x_i) - \frac{1}{N_2} \sum_{i=1}^{N_2} \psi_m(y_i) \right)^2 := \sum_{m=1}^{\infty} \gamma_m a_m^2.$$

Our goal is to show that (a) $a_m \sim \mathcal{N}(0, (N\rho_1\rho_2)^{-1})$, for $\forall m$, and (b) a_m and a_n are independent when $m \neq n$.

First note that

$$\mathbb{E}(a_m) = \mathbb{E} \left(\frac{1}{N_1} \sum_{i=1}^{N_1} \psi_m(x_i) - \frac{1}{N_2} \sum_{i=1}^{N_2} \psi_m(y_i) \right) = 0.$$

In addition we have,

$$\begin{aligned}
Cov(a_m, a_n) &= \mathbb{E}(a_m a_n) - \mathbb{E}(a_m) \mathbb{E}(a_n) \\
&= \mathbb{E}(a_m a_n) \\
&= \mathbb{E} \left(\frac{1}{N_1} \sum_{i=1}^{N_1} \psi_m(x_i) - \frac{1}{N_2} \sum_{i=1}^{N_2} \psi_m(y_i) \right) \left(\frac{1}{N_1} \sum_{i=1}^{N_1} \psi_n(x_i) - \frac{1}{N_2} \sum_{i=1}^{N_2} \psi_n(y_i) \right) \\
&= \mathbb{E}_X \left(\frac{1}{N_1^2} \sum_{i=1}^{N_1} \psi_m(x_i) \psi_n(x_i) \right) + \mathbb{E}_Y \left(\frac{1}{N_2^2} \sum_{i=1}^{N_2} \psi_m(y_i) \psi_n(y_i) \right) \\
&= \frac{1}{\rho_1 N} \mathbb{E}_X \left(\frac{1}{N_1} \sum_{i=1}^{N_1} \psi_m(x_i) \psi_n(x_i) \right) + \frac{1}{\rho_2 N} \mathbb{E}_Y \left(\frac{1}{N_2} \sum_{i=1}^{N_2} \psi_m(y_i) \psi_n(y_i) \right) \\
&= \frac{1}{N} \left[\frac{1}{\rho_1} \int_{\mathcal{H}} \psi_m(x) \psi_n(x) d(\tilde{\eta} \# P)(x) + \frac{1}{\rho_2} \int_{\mathcal{H}} \psi_m(y) \psi_n(y) d(\tilde{\eta} \# Q)(y) \right] \\
&= \frac{1}{N \rho_1 \rho_2} \int_{\mathcal{H}} \psi_m(z) \psi_n(z) dR(z) \\
&= \frac{1}{N \rho_1 \rho_2} \delta_{mn}.
\end{aligned}$$

An application of CLT follows that (a) holds. This together with vanishing covariance proves (b). Consequently, we can apply the CLT for degenerate V-statistics [40, Section 5.5.2] to obtain the limiting distribution, with $A_m \sim \mathcal{N}(0, 1)$,

$$N \|\hat{C}_{\eta \# P} - \hat{C}_{\eta \# Q}\|_{\mathcal{H}}^2 \sim \sum_{m=1}^{\infty} \frac{\gamma_m}{\rho_1 \rho_2} A_m^2.$$

Let us now look at the difference between this V-statistic and our U-statistic, i.e. $\hat{\mathbb{T}}$ in (A.5). We see that

$$\begin{aligned}
\|\hat{C}_{\eta \# P} - \hat{C}_{\eta \# Q}\|_{\mathcal{H}}^2 - \hat{\mathbb{T}} &= \frac{1}{N_1^2} \sum_{i,j} \langle x_i, x_j \rangle_{\mathcal{H}} + \frac{1}{N_2^2} \sum_{i,j} \langle y_i, y_j \rangle_{\mathcal{H}} - \frac{2}{N_1 N_2} \sum_{i,j} \langle x_i, y_j \rangle_{\mathcal{H}} \\
&\quad - \frac{1}{N_1(N_1-1)} \sum_{i,j; i \neq j} \langle x_i, x_j \rangle_{\mathcal{H}} + \frac{1}{N_2(N_2-1)} \sum_{i,j; i \neq j} \langle y_i, y_j \rangle_{\mathcal{H}} + \frac{2}{N_1 N_2} \sum_{i,j} \langle x_i, y_j \rangle_{\mathcal{H}} \\
&= - \left[\frac{1}{N_1(N_1-1)} - \frac{1}{N_1^2} \right] \sum_{i,j; i \neq j} \langle x_i, x_j \rangle_{\mathcal{H}} - \left[\frac{1}{N_2(N_2-1)} - \frac{1}{N_2^2} \right] \sum_{i,j; i \neq j} \langle y_i, y_j \rangle_{\mathcal{H}} \\
&\quad + \left(\frac{1}{N_1^2} \sum_{i=1}^{N_1} \|x_i\|_{\mathcal{H}}^2 + \frac{1}{N_2^2} \sum_{i=1}^{N_2} \|y_i\|_{\mathcal{H}}^2 \right) \\
&= -K^x - K^y + B.
\end{aligned}$$

We claim that $K^x = O_p(N_1^{-2})$, $K^y = O_p(N_2^{-2})$, and $NB \xrightarrow{P} \sum_{m=1}^{\infty} \gamma_m (\rho_1 \rho_2)^{-1}$. As a result,

$$\begin{aligned}
N \left[\|\hat{C}_{\eta \# P} - \hat{C}_{\eta \# Q}\|_{\mathcal{H}}^2 - \hat{\mathbb{T}} \right] &= -N O_p(N_1^{-2}) - N O_p(N_2^{-2}) + \sum_{m=1}^{\infty} \frac{\gamma_m}{\rho_1 \rho_2} + o_p(1) \\
&= \sum_{m=1}^{\infty} \frac{\gamma_m}{\rho_1 \rho_2} + o_p(1),
\end{aligned}$$

so that $N\hat{\mathbb{T}} \sim \sum_{m=1}^{\infty} \gamma_m (\rho_1 \rho_2)^{-1} (A_m^2 - 1)$, and we conclude the proof by reassigning $\gamma_m \leftarrow \gamma_m (\rho_1 \rho_2)^{-1}$ to obtain (A.3).

Proof of Claim. For the K -terms we have

$$\begin{aligned} K^x &= \left[\frac{1}{N_1(N_1-1)} - \frac{1}{N_1^2} \right] \sum_{i,j;i \neq j} \langle x_i, x_j \rangle_{\mathcal{H}} \\ &= \frac{1}{N_1^2(N_1-1)} \sum_{i,j;i \neq j} \langle x_i, x_j \rangle_{\mathcal{H}} \\ &= \sum_{m=1}^{\infty} \gamma_m \frac{1}{N_1} \frac{1}{N_1(N_1-1)} \sum_{i,j;i \neq j} \psi_m(x_i) \psi_m(x_j) \\ &= \sum_{m=1}^{\infty} \gamma_m K_m^x, \end{aligned}$$

where K_m^x is defined as the inner sum. Since $\mathbb{E}_X \psi_m(x) = 0$, we have $\mathbb{E}_X(K_m^x) = \frac{1}{N_1} [\mathbb{E}_X \psi_m(x)]^2 = 0$, and

$$\begin{aligned} \text{Var}_X(K_m^x) &= \mathbb{E}_X[(K_m^x)^2] \\ &= \frac{1}{N_1^2} \mathbb{E}_X \left[\frac{1}{N_1^2(N_1-1)^2} \sum_{i \neq j} \sum_{l \neq k} \psi_m(x_i) \psi_m(x_j) \psi_m(x_l) \psi_m(x_k) \right] \end{aligned} \quad (\text{A.6})$$

$$\begin{aligned} &= \frac{1}{N_1^2} \mathbb{E}_X \left[\frac{1}{N_1^2(N_1-1)^2} \sum_{i \neq j} \psi_m^2(x_i) \psi_m^2(x_j) \right] \\ &= \frac{1}{N_1^2} \cdot \frac{1}{N_1(N_1-1)} (\mathbb{E}_X[\psi_m^2(x)])^2. \end{aligned} \quad (\text{A.7})$$

The cross terms—terms involving $l \neq i$ or $k \neq j$ —vanish due to the sample being iid and eigenfunctions having zero expectations. The expectation in the last line is finite by assumption (ii), so that $\text{Var}_X(K_m^x) = O(N_1^{-4})$, giving $K_m^x = O_p(N_1^{-2})$. Note that the assumption (ii) moreover implies the convergence of the big-oh coefficients, leading to $K^x = \sum_{m=1}^{\infty} \gamma_m K_m^x = O_p(N_1^{-2})$. Similarly we get $K^y = O_p(N_2^{-2})$.

For the term B , we have

$$B = \frac{1}{N_1^2} \sum_{i=1}^{N_1} \|x_i\|_{\mathcal{H}}^2 + \frac{1}{N_2^2} \sum_{i=1}^{N_2} \|y_i\|_{\mathcal{H}}^2 = \sum_{m=1}^{\infty} \gamma_m \left[\frac{1}{N_1^2} \sum_{i=1}^{N_1} \psi_m^2(x_i) + \frac{1}{N_2^2} \sum_{i=1}^{N_2} \psi_m^2(y_i) \right] := \sum_{m=1}^{\infty} \gamma_m C_m.$$

Taking expectation,

$$\begin{aligned} \mathbb{E}_{X,Y}(C_m) &= \frac{1}{\rho_1 N} \int_{\mathcal{H}} \psi_m^2(x) d(\tilde{\eta} \# P)(x) + \frac{1}{\rho_2 N} \int_{\mathcal{H}} \psi_m^2(y) d(\tilde{\eta} \# Q)(y) \\ &= \frac{1}{N \rho_1 \rho_2} \int_{\mathcal{H}} \psi_m^2(z) dR(z) \\ &= \frac{1}{N \rho_1 \rho_2}. \end{aligned}$$

Thus $\mathbb{E}_{X,Y}(NB) = \sum_m \gamma_m (\rho_1 \rho_2)^{-1}$. Finally,

$$NB = \sum_{m=1}^{\infty} \gamma_m \left[\frac{1}{\rho_1 N_1} \sum_{i=1}^{N_1} \psi_m^2(x_i) + \frac{1}{\rho_2 N_2} \sum_{i=1}^{N_2} \psi_m^2(y_i) \right] \xrightarrow{P} \sum_{m=1}^{\infty} \gamma_m \left[\frac{1}{\rho_1} \mathbb{E}_X \psi_m^2(x) + \frac{1}{\rho_2} \mathbb{E}_Y \psi_m^2(y) \right] = \mathbb{E}_{X,Y}(NB)$$

by the weak law of large numbers. This proves the claim for B .

Alternative Distribution. For the the limiting distribution under H_1 , notice that the first two terms in (A.2) are the one-sample U-statistic calculated on the samples $\{\mu_i\}_{i=1}^{N_1}$ and $\{\nu_i\}_{i=1}^{N_2}$, respectively. Using the CLT for non-degenerate U-statistics [40, Section 5.5.1, Theorem A], we have

$$\begin{aligned} \sqrt{N_1} \left[\frac{\sum_{i,j:i \neq j} \langle \eta(\mu_i), \eta(\mu_j) \rangle_{\mathcal{H}}}{N_1(N_1-1)} - \mathbb{E}_{\mu, \mu' \sim P} \langle \eta(\mu), \eta(\mu') \rangle_{\mathcal{H}} \right] &\rightsquigarrow N(0, 4\mathbb{V}_{\mu \sim P} [\mathbb{E}_{\mu' \sim P} \langle \eta(\mu), \eta(\mu') \rangle_{\mathcal{H}}]), \\ \sqrt{N_2} \left[\frac{\sum_{i,j:i \neq j} \langle \eta(\nu_i), \eta(\nu_j) \rangle_{\mathcal{H}}}{N_2(N_2-1)} - \mathbb{E}_{\nu, \nu' \sim Q} \langle \eta(\nu), \eta(\nu') \rangle_{\mathcal{H}} \right] &\rightsquigarrow N(0, 4\mathbb{V}_{\nu \sim Q} [\mathbb{E}_{\nu' \sim Q} \langle \eta(\nu), \eta(\nu') \rangle_{\mathcal{H}}]). \end{aligned}$$

For the third summand, using an equivalent CLT for two-sample U-statistic [16, Theorem 2.1],

$$\begin{aligned} \sqrt{N} \left[\frac{\sum_{i,j} \langle \eta(\mu_i), \eta(\nu_j) \rangle_{\mathcal{H}}}{N_1 N_2} - \mathbb{E}_{\mu \sim P, \nu \sim Q} \langle \eta(\mu), \eta(\nu) \rangle_{\mathcal{H}} \right] &\rightsquigarrow \\ N \left(0, \frac{1}{\rho_1} \mathbb{V}_{\mu \in P} [\mathbb{E}_{\nu \sim Q} \langle \eta(\mu), \eta(\nu) \rangle_{\mathcal{H}}] + \frac{1}{\rho_2} \mathbb{V}_{\nu \in Q} [\mathbb{E}_{\mu \sim P} \langle \eta(\mu), \eta(\nu) \rangle_{\mathcal{H}}] \right). \end{aligned}$$

We obtain (A.4) by combining the above three results. \square

The following result now ensures that approximations of $\hat{\mathbb{T}}$ using the top few eigenfunctions and a finite number of CDF embeddings can be constructed with small approximation errors, provided the manifold eigenvalues are declining suitably fast and the finite dimensional $\eta_D(\cdot)$ is suitably smooth.

Proposition 10. *Suppose that (i), (ii) and (iii) hold. Then we have $\sqrt{N}(\hat{\mathbb{T}} - \hat{\mathbb{T}}_{L_N}) = o_p(1)$ and $\sqrt{N}(\hat{\mathbb{T}}_{L_N} - \tilde{\mathbb{T}}_{L_N, D_N}) = o_p(1)$ for the following choices of L_N, D_N :*

$$L_N \geq \min_{L'} \left\{ L' : \sum_{\ell=L'+1}^{\infty} \alpha_{\ell} \lambda_{\ell}^{(n+3)/2} \leq \frac{1}{N^{1+\delta}} \right\}, \quad D_N \geq kc^2 N^{1+\delta} \sum_{\ell=1}^{L_N} \alpha_{\ell} \lambda_{\ell}^{(n-1)/2},$$

where $\delta, k > 0$ are constants depending only on \mathcal{X} .

As we mention in the discussion after condition (i), for the heat kernel with tuning parameter t : $\alpha(\lambda) = \exp(-t\lambda)$, the assumption (i) that $\sum_{\ell=1}^{\infty} \alpha_{\ell} \lambda_{\ell}^{(n+3)/2} < \infty$ holds. The bound on D_N is a consequence of classical bounds on Riemann sum approximation errors in terms of $\|\eta'\|_{\infty}$. Absolute continuity of $\mu \sim P, \nu \sim Q$ ensures the existence of $(F_{\phi_{\ell}^{\sharp}\mu}^{-1})'(s), (F_{\phi_{\ell}^{\sharp}\nu}^{-1})'(s)$ (where prime denotes the derivative) for Lebesgue-almost every $s \in [0, 1]$ [18, Lemma 2.3].

Proof. Notice that given L_N , summands in the expression $\hat{\mathbb{T}} - \hat{\mathbb{T}}_{L_N}$ are the tail sums $\sum_{\ell=L_N+1}^{\infty} \alpha_{\ell} \mathcal{W}_2^2(\phi_{\ell}^{\sharp}\cdot, \phi_{\ell}^{\sharp}\cdot)$ starting at the $L_N + 1^{\text{th}}$ term. Using a similar approach as the proof of Proposition 7, this is bounded above by a scalar multiple of the geodesic distance, specifically $c\mathcal{W}_2^{\mathcal{X}}(\cdot, \cdot) \sqrt{\sum_{\ell=L_N+1}^{\infty} \alpha_{\ell} \lambda_{\ell}^{(n+3)/2}}$. By assumption $\sum_{\ell=1}^{\infty} \alpha_{\ell} \lambda_{\ell}^{(n+3)/2} < \infty$, so that given $\epsilon > 0$ we can always choose a starting point to make the tail sum $< \epsilon$. The choice of L_N follows by taking $\epsilon = N^{-(1+\delta)}$.

To obtain the choice of D_N , we first use a similar approach to the proof of Proposition 9 to simplify $\tilde{\mathbb{T}}_{L,D'}$ for any L, D' :

$$\begin{aligned} \tilde{\mathbb{T}}_{L,D'} = \sum_{\ell=1}^L & \left[\frac{1}{N_1(N_1-1)} \sum_{i,j:i \neq j} \eta_{D'}(\phi_{\ell} \# \mu_i)^T \eta_{D'}(\phi_{\ell} \# \mu_j) + \frac{1}{N_2(N_2-1)} \sum_{i,j:i \neq j} \eta_{D'}(\phi_{\ell} \# \nu_i)^T \eta_{D'}(\phi_{\ell} \# \nu_j) \right. \\ & \left. - \frac{2}{N_1 N_2} \sum_{i,j} \eta_{D'}(\phi_{\ell} \# \mu_i)^T \eta_{D'}(\phi_{\ell} \# \nu_j) \right]. \end{aligned} \quad (\text{A.8})$$

Recall that the inverse CDF transformation induced by $\eta_0(\phi_{\ell} \# \mu) \equiv F_{\phi_{\ell} \# \mu}^{-1}$ maps $[0, 1]$ to a bounded interval that is the range of ϕ_{ℓ} , and $\|\phi_{\ell}\|_{\infty} \leq c \lambda_{\ell}^{(n-1)/4}$ using Hörmander's bound on the supremum norm of the eigenfunctions. Using classical results on Riemann sum approximation errors [4, 13] we thus have for any ℓ :

$$|\alpha_{\ell} \langle \eta_0(\phi_{\ell} \# \mu), \eta_0(\phi_{\ell} \# \nu) \rangle_{\mathcal{H}} - \eta_{D'}(\phi_{\ell} \# \mu)^T \eta_{D'}(\phi_{\ell} \# \nu)| \leq \frac{k}{D'} \alpha_{\ell} \left\| (F_{\phi_{\ell} \# \mu}^{-1} F_{\phi_{\ell} \# \nu}^{-1})' \right\|_{\infty} \leq \frac{2k c^2}{D'} \alpha_{\ell} \lambda_{\ell}^{(n-1)/2}.$$

Given $L = L_N$, we simply choose $D' = D_N$ large enough to make the right hand side above smaller than $N^{-(1+\delta)}$. While it is possible to make the upper bound tighter using recent results (such as [13]), the above coarser bound suffices for our purpose. \square

We now state a version of Theorem 2 in the main paper, with specifications for $\gamma_m, \sigma_1^2, L_N, D_N$ now available through the above two results.

Theorem 2. *Assume conditions (i)-(iii) hold. Define $N = N_1 + N_2$, and suppose that as $N_1, N_2 \rightarrow \infty$, we have $N_1/N \rightarrow \rho_1, N_2/N \rightarrow \rho_2 = 1 - \rho_1$, for some fixed $0 < \rho_1 < 1$. With $L \geq L_N, D' \geq D_N$ chosen per Proposition 10, under $H_0 : C_{\eta \# P} = C_{\eta \# Q}$ we have*

$$N \tilde{\mathbb{T}}_{L,D'} \sim \sum_{m=1}^{\infty} \gamma_m (A_m^2 - 1),$$

where A_m, γ_m are defined as in Proposition 9. Further, under $H_1 : C_{\eta \# P} \neq C_{\eta \# Q}$ we have $\sqrt{N} (\tilde{\mathbb{T}}_{L,D'} - \mathbb{T}) \sim N(0, \sigma_1^2)$.

Proof. This a combination of Propositions 9 and 10, and Slutsky's theorem. \square

We conclude with a proof of Theorem 3, which gives power guarantee of the test based on $\tilde{\mathbb{T}}_{L,D'}$ for contiguous alternatives.

Theorem 3. *Assume conditions (i)-(iii) hold, and let L, D' be chosen as in Theorem 2. Then for the sequence of contiguous alternatives H_{1N} such that $N \|\delta_N\|_{\mathcal{H}^*}^2 \rightarrow \infty$, the level- α test based on $\tilde{\mathbb{T}}_{L,D'}$ is consistent for any $\alpha \in (0, 1)$, that is as $N \rightarrow \infty$ the asymptotic power approaches 1.*

Proof. It is enough the prove consistency using $\hat{\mathbb{T}}$, as the difference between $\hat{\mathbb{T}}$ and $\tilde{\mathbb{T}}_{L,D'}$ is negligible by choice of L, D' . To do so we utilize proof techniques similar to [21, Theorem 13]. Define $c_N := N^{1/2} \|\delta_N\|_{\mathcal{H}}$, and expand the simplified centered version of the test statistic in (A.5)

but under H_1 so that the centering terms do not cancel out:

$$\begin{aligned}\hat{\mathbb{T}}_c = & \frac{1}{N_1(N_1-1)} \sum_{i,j:i \neq j} \langle \eta(\mu_i) - C_{\eta \# P}, \eta(\mu_j) - C_{\eta \# P} \rangle_{\mathcal{H}} \\ & + \frac{1}{N_2(N_2-1)} \sum_{i,j:i \neq j} \langle \eta(\nu_i) - C_{\eta \# Q}, \eta(\nu_j) - C_{\eta \# Q} \rangle_{\mathcal{H}} \\ & - \frac{2}{N_1 N_2} \sum_{i,j} \langle \eta(\mu_i) - C_{\eta \# P}, \eta(\nu_j) - C_{\eta \# Q} \rangle_{\mathcal{H}} \end{aligned} \quad (\text{A.9})$$

The centered pushforwards have the same Hilbert centroids, thus as $N \rightarrow \infty$ by Proposition 9,

$$N\hat{\mathbb{T}}_c \rightsquigarrow \sum_{m=1}^{\infty} \gamma_m (A_m^2 - 1) := S.$$

Subtracting $\hat{\mathbb{T}}_c$ from $\hat{\mathbb{T}}$ and its expansion in Eq. (A.2) on the left and right hand respectively, then simplifying we have

$$\begin{aligned}N(\hat{\mathbb{T}} - \hat{\mathbb{T}}_c) &= N \left[-\frac{1}{N_1} \sum_{i=1}^{N_1} \langle \delta_N, \eta(\mu_i) - C_{\eta \# P} \rangle_{\mathcal{H}} + \frac{1}{N_2} \sum_{i=1}^{N_2} \langle \delta_N, \eta(\nu_i) - C_{\eta \# Q} \rangle_{\mathcal{H}} + \frac{\langle \delta_N, \delta_N \rangle_{\mathcal{H}}}{2} \right] \\ &= N \left[\frac{\|\delta_N\|_{\mathcal{H}}}{N_1} \sum_{i=1}^{N_1} \left\langle \frac{\delta_N}{\|\delta_N\|_{\mathcal{H}}}, \eta(\mu_i) - C_{\eta \# P} \right\rangle_{\mathcal{H}} \right. \\ &\quad \left. - \frac{\|\delta_N\|_{\mathcal{H}}}{N_2} \sum_{i=1}^{N_2} \left\langle \frac{\delta_N}{\|\delta_N\|_{\mathcal{H}}}, \eta(\nu_i) - C_{\eta \# Q} \right\rangle_{\mathcal{H}} + \frac{\|\delta_N\|_{\mathcal{H}}^2}{2} \right]. \end{aligned} \quad (\text{A.10})$$

Given N the inner products $\langle \delta_N / \|\delta_N\|_{\mathcal{H}}, \eta(\mu_i) - C_{\eta \# P} \rangle_{\mathcal{H}}$ are i.i.d. random variables with mean 0, so by CLT then using $\|\delta_N\|_{\mathcal{H}} = c_N N^{-1/2}$ we get

$$\frac{1}{\sqrt{N_1}} \sum_{i=1}^{N_1} \left\langle \frac{\delta_N}{\|\delta_N\|_{\mathcal{H}}}, \eta(\mu_i) - C_{\eta \# P} \right\rangle_{\mathcal{H}} \rightsquigarrow U \quad \Rightarrow \quad \frac{N \|\delta_N\|_{\mathcal{H}}}{N_1} \sum_{i=1}^{N_2} \left\langle \frac{\delta_N}{\|\delta_N\|_{\mathcal{H}}}, \eta(\nu_i) - C_{\eta \# Q} \right\rangle_{\mathcal{H}} \rightsquigarrow \frac{c_N}{\sqrt{\rho_1}} U,$$

where U is the zero mean Gaussian random variable that is the limiting distribution of the above inner product sum. Similarly we have

$$\frac{N \|\delta_N\|_{\mathcal{H}}}{N_2} \sum_{i=1}^{N_2} \left\langle \frac{\delta_N}{\|\delta_N\|_{\mathcal{H}}}, \eta(\nu_i) - C_{\eta \# Q} \right\rangle_{\mathcal{H}} \rightsquigarrow \frac{c_N}{\sqrt{\rho_2}} V,$$

where V is also Gaussian, zero mean, and independent of U . Putting everything together in the right hand side of (A.10), and using $\|\delta_N\|_{\mathcal{H}} = c_N N^{-1/2}$, given the threshold t_{α} for a level- α test

$$P_{H_N} \left(N\hat{\mathbb{T}} > t_{\alpha} \right) \rightarrow P \left[S + c_N \left(\frac{U}{\sqrt{\rho_1}} - \frac{V}{\sqrt{\rho_2}} \right) + \frac{c_N^2}{2} > t_{\alpha} \right].$$

By assumption $c_N^2 \rightarrow \infty$, so the asymptotic power approaches 1 as $N \rightarrow \infty$. \square

A.4 Proofs and Notes for Section 4.2

To guarantee size control when using the the harmonic mean p -value we establish a version of Theorem 1 from [28]. Assume that a test statistic $Z \in \mathbb{R}^D$ has null distribution with zero mean and every pair of coordinates of Z follows bivariate Gaussian distribution. Compute the coordinate-wise two-sided p -values $p_k = 2(1 - \Phi(|Z_k|))$ where Φ is the standard Gaussian CDF.

Theorem 4. *Let $p_k, k = 1, \dots, D$ be the null p -values as above and p^H computed via harmonic mean approach, then*

$$\lim_{\alpha \rightarrow 0} \frac{\text{Prob}\{p^H \leq \alpha\}}{\alpha} = 1.$$

Proof. The proof of Theorem 1 from [28] hinges on Lemma 3 in their supplemental material. We show that Lemma 3 holds for the harmonic mean combination method. Note that the multiplication by π present in Lemma 3 cancels out when inverse cotangent with a multiplier of $1/\pi$ is applied later on; so it is not relevant to the flow of the proof.

To this end, consider the functions $p(x) = 2(1 - \Phi(|x|))$ and $h(x) = 1/p(x)$. We need to prove the following three statements:

(1) for any $|x| > \Phi^{-1}(3/4)$,

$$\frac{\cos[p(x)\pi]}{p(x)} \leq h(x) \leq \frac{1}{p(x)}$$

(2) For any constant $0 < |a| < 1$, we have

$$\lim_{x \rightarrow +\infty} \frac{h(x)}{x^2 h(ax)} > c_a > 0,$$

where c_a is some constant only dependent on a .

(3) Suppose that X_0 has standard normal distribution, then we have

$$P\{h(X_0) \geq t\} = \frac{1}{t} + O(1/t^3).$$

Statement (1) is trivial, as $h(x) = 1/p(x)$ by definition and the cosine function is upper bounded by one. Statement (2) holds by the same argument as in the supplement of [28]. Statement (3) follows from the fact that when X_0 is standard normal, then $p(x)$ is a null p -value, and so

$$P\{h(X_0) \geq t\} = P\{p(X_0) \leq 1/t\} = \frac{1}{t}.$$

Note that there is no $O(1/t^3)$ term at all, but we kept the form of the statement the same as in [28].

Now, the proof of Theorem 1 from [28] with weights $\omega_k = 1/D, k = 1, 2, \dots, D$ goes through to give

$$P\left\{\frac{1}{D} \sum \frac{1}{p_k} \geq t\right\} = \frac{1}{t} + o(1/t).$$

Note that $p^H = H\left(D/\left(\frac{1}{p_1} + \frac{1}{p_2} + \dots + \frac{1}{p_D}\right)\right)$, where the function H has a known form described in [44] and satisfies $H(x)/x \rightarrow 1$ as $x \rightarrow 0$. Thus, as $\alpha \rightarrow 0$, we have

$$P\{p^H \leq \alpha\} \asymp P\left\{\frac{1}{D} \sum \frac{1}{p_k} \geq 1/\alpha\right\} \asymp \frac{1}{1/\alpha} + o\left(\frac{1}{1/\alpha}\right) \asymp \alpha.$$

□

B Implementation of Testing on Graphs

Here we provide an R implementation for the Chicago Crime example for the “Theft” category. This code and relevant data can be obtained by downloading the gzipped tar (.tar.gz) source of this paper from arxiv.

```

library(data.table)
library(harmonicmeanp)
library(Matrix)
library(RSpectra)
library(sf)
library(spdep)

#parameters for approximate Hilbert embedding
evec_cnt = 20 #L in paper
invCDFnsamples = 5 #Dprime in paper

#load subset of Chicago crime data
load("chicago_theft2018.RData")
#data contents:
#beat_map --- map of beats (geographic area subdivision used by police)
#distros --- contains three matrices (Tuesday, Thursday, and Saturday)
#each matrix row corresponds to a day in 2018, each column corresponds to a beat
#the values give the row-normalized counts of Theft crime for day & beat
#thus, each matrix row is a probability distribution on the beat graph

#adjacency matrix for the underlying graph
#graph nodes are beats, edges capture whether the beats share a boundary
A = nb2mat(poly2nb(as(beat_map, "Spatial")), style="B", zero.policy = TRUE)
#Laplacian matrix
D = Diagonal(x = rowSums(A))
Lap = D - A

#eigendecomposition
ev = eigs(Lap, k=evec_cnt+1, which = "SM")
#drop the constant eigenvector with zero eigenvalue & reorder
evals = ev$values[evec_cnt:1]
evecs = ev$vectors[,evec_cnt:1]

#approximate Hilbert embedding for a probability distribution on the graph
#a distribution is represented as a vector of weights with sum=1
#we use rolling joins to efficiently compute the quantiles
approx_hilbert_emb <- function(wts, Dprime, lambda, phi){
  L = ncol(phi) #number of eigenvectors
  alpha = 1/lambda**2 #biharmonic scaling

  #quantiles to be extracted, for each eigenvector
  q = CJ(ell=1:L, s_k=(1:Dprime)/(Dprime+1))
  setkey(q, "ell", "s_k")

  #compute pushforward by each eigenvector
  df = data.table(x=as.numeric(phi), wt=rep(wts, L),
                  ell = rep(1:L, each=length(wts)))
  df = df[,.(wt=sum(wt)), keyby=(ell, x)] #aggregate & sort

  #quantile definition has strict inequality, so subtract eps
  eps = 1e-8
  df = df[, s_k:=cumsum(wt)/sum(wt)-eps, by=ell]
  setkey(df, "ell", "s_k")
}

```

```

#extract quantiles via rolling join for all eigenvectors at once
df[q,,roll=-Inf][order(ell,s_k)][, x:=sqrt(alpha[ell]/Dprime)*x]$x
}

#approximate Hilbert embeddings for all distributions (=rows of the matrix)
embed_all_rows <- function(R, ...){
  do.call('rbind', lapply(seq_len(nrow(R)),
    function(i) approx_hilbert_emb(R[i,], ...)))
}

combo_test <- function(E1, E2){
  #t-test on each dimension of the Hilbert embedding
  p_ttests = sapply(seq_len(ncol(E1)), function(i)
    tryCatch({t.test(E1[, i], E2[, i])$p.value}, error=function(e){NaN}))
  if(all(is.nan(p_ttests))){  

    stop("data are essentially constant")  

  } else {  

    #NaN values provide no information towards acceptance/rejection  

    p_ttests = p_ttests[!is.nan(p_ttests)]  

    #overall p-value using harmonic mean combo  

    unname(p.hmp(p_ttests, L=length(p_ttests), multilevel=FALSE))  

  }
}

ETue = embed_all_rows(distros$Tuesday, invCDFnsamples, evals, evecs)
ETHu = embed_all_rows(distros$Thursday, invCDFnsamples, evals, evecs)
ESat = embed_all_rows(distros$Saturday, invCDFnsamples, evals, evecs)

cat("Tuesday vs Thursday:", combo_test(ETue, ETHu), "\n") #0.4518086
cat("Tuesday vs Saturday:", combo_test(ETue, ESat), "\n") #4.728311e-06

```

C Additional numerical results

Table 5 shows the outputs for the other 8 competing methods from the R package fdANOVA for the finite intervals synthetic data setting (Section 5 of the main document). See <https://www.rdocumentation.org/packages/fdANOVA/versions/0.1.2/topics/fanova.tests> for full names of all methods.

δ	CH	CS	L2N	L2b	FN	FB	Fb	GPF
0	0.031	0.03	0.033	0.024	0.031	0.028	0.033	0.026
0.1	0.025	0.024	0.03	0.044	0.027	0.03	0.041	0.021
0.2	0.026	0.029	0.037	0.06	0.033	0.034	0.058	0.025
0.3	0.036	0.041	0.044	0.067	0.041	0.04	0.067	0.033
0.4	0.034	0.035	0.036	0.057	0.034	0.035	0.056	0.032
0.5	0.051	0.052	0.058	0.091	0.056	0.057	0.088	0.044
0.6	0.056	0.066	0.066	0.089	0.061	0.066	0.088	0.051
0.7	0.07	0.083	0.083	0.121	0.084	0.081	0.119	0.064
0.8	0.085	0.097	0.095	0.151	0.093	0.094	0.144	0.081
0.9	0.118	0.142	0.14	0.2	0.144	0.137	0.194	0.118
1	0.158	0.182	0.176	0.232	0.183	0.173	0.228	0.154
1.1	0.215	0.247	0.246	0.303	0.251	0.242	0.301	0.212
1.2	0.27	0.31	0.303	0.375	0.311	0.3	0.368	0.27
1.3	0.328	0.363	0.357	0.438	0.37	0.353	0.43	0.324
1.4	0.395	0.432	0.432	0.504	0.436	0.423	0.499	0.394
1.5	0.488	0.52	0.514	0.592	0.521	0.511	0.586	0.483
1.6	0.534	0.595	0.576	0.652	0.593	0.566	0.647	0.544
1.7	0.628	0.677	0.669	0.723	0.678	0.661	0.719	0.631
1.8	0.704	0.737	0.727	0.789	0.748	0.725	0.785	0.707
1.9	0.785	0.823	0.812	0.869	0.827	0.806	0.867	0.793
2	0.83	0.849	0.844	0.88	0.85	0.841	0.875	0.832
2.1	0.865	0.888	0.881	0.916	0.887	0.878	0.915	0.872
2.2	0.903	0.922	0.916	0.946	0.928	0.912	0.946	0.907
2.3	0.938	0.95	0.944	0.964	0.951	0.944	0.963	0.944
2.4	0.958	0.973	0.967	0.977	0.972	0.966	0.976	0.964
2.5	0.974	0.98	0.976	0.985	0.981	0.975	0.985	0.974
2.6	0.977	0.981	0.979	0.987	0.981	0.978	0.986	0.977
2.7	0.989	0.996	0.992	0.997	0.996	0.992	0.997	0.991
2.8	0.997	0.998	0.997	0.998	0.998	0.997	0.998	0.996
2.9	0.996	0.997	0.996	0.999	0.997	0.996	0.999	0.997
3	0.998	1	0.999	1	1	0.999	1	0.999

Table 5: Outputs for other methods in the functional curves synthetic data setting.